Linked alterations in gray and white matter morphology in adults with high-functioning autism spectrum disorder: A multimodal brain imaging study

Takashi Itahashi[a,b], Takashi Yamada[c], Motoaki Nakamura[c,d], Hiromi Watanabe[c], Bun Yamagata[c], Daiki Jimbo[e], Seiji Shioda[e], Miho Kuroda[c,f,g], Kazuo Toriizuka[a], Nobumasa Kato[b], Ryuichiro Hashimoto[b,h,*]

[a]Department of Pharmacognosy and Phytochemistry, Showa University School of Pharmacy, Tokyo, Japan
[b]Medical Institute of Developmental Disabilities Research, Showa University, Tokyo, Japan
[c]Department of Psychiatry, Showa University School of Medicine, Tokyo, Japan
[d]Kinko Hospital, Kanagawa Psychiatric Center, Kanagawa, Japan
[e]Department of Anatomy, Showa University School of Medicine, Tokyo, Japan
[f]Child Mental Health-care Center, Fukushima University, Fukushima, Japan
[g]Department of Child Neuropsychiatry, Graduate School of Medicine, The University of Tokyo, Tokyo, Japan
[h]Department of Language Sciences, Graduate School of Humanities, Tokyo Metropolitan University, Tokyo, Japan

ARTICLE INFO

ABSTRACT

Growing evidence suggests that a broad range of behavioral anomalies in people with autism spectrum disorder (ASD) can be linked with morphological and functional alterations in the brain. However, the neuroanatomical underpinnings of ASD have been investigated using either structural magnetic resonance imaging (MRI) or diffusion tensor imaging (DTI), and the relationships between abnormalities revealed by these two modalities remain unclear. This study applied a multimodal data-fusion method, known as linked independent component analysis (ICA), to a set of structural MRI and DTI data acquired from 46 adult males with ASD and 46 matched controls in order to elucidate associations between different aspects of atypical neuroanatomy of ASD. Linked ICA identified two composite components that showed significant between-group differences, one of which was significantly correlated with age. In the other component, participants with ASD showed decreased gray matter (GM) volumes in multiple regions, including the bilateral fusiform gyri, bilateral orbitofrontal cortices, and bilateral pre- and post-central gyri. These GM changes were linked with a pattern of decreased fractional anisotropy (FA) in several white matter tracts, such as the bilateral inferior longitudinal fasciculi, bilateral inferior fronto-occipital fasciculi, and bilateral corticospinal tracts. Furthermore, unimodal analysis for DTI data revealed significant reductions of FA along with increased mean diffusivity in those tracts for ASD, providing further evidence of disrupted anatomical connectivity. Taken together, our findings suggest that, in ASD, alterations in different aspects of brain morphology may co-occur in specific brain networks, providing a comprehensive view for understanding the neuroanatomy of this disorder.

1. Introduction

Recent magnetic resonance imaging (MRI) studies have examined multiple aspects of structural abnormalities in the brain of autism spectrum disorder (ASD), including gray matter (GM) density, cortical thickness, and white matter (WM) microstructures (e.g., Barnea-Goraly et al., 2010; Ecker et al., 2013; Hadjikhani et al., 2006; Kosaka et al., 2010). Among several others, voxel-based morphometry (VBM) is perhaps one of the most widely used methods for evaluating GM alterations and, using this methodology, volumetric abnormalities have been revealed in various regions in the ASD brain (Boddaert et al., 2004; Bonilha et al., 2008; Ecker et al., 2012; Greimel et al., 2013; Hyde et al., 2010; Kosaka et al., 2010; McAlonan et al., 2008; Rojas et al., 2006; Waiter et al., 2004). These regions include the bilateral fusiform gyri, bilateral hippocampus, right amygdala, right insula, right inferior frontal gyrus, and cerebellum (see Cauda et al., 2011; Duerden et al., 2012; for review); many of these regions are thought to play crucial roles for social, cognitive, and affective functions that are profoundly impaired in ASD.

On the other hand, atypical WM microstructure in people with ASD has been examined using diffusion tensor imaging (DTI), a technique

* Corresponding author at: Medical Institute of Developmental Disabilities Research, Showa University, 6-11-11, Kita-karasuyama, Setagaya-ku, Tokyo 157-8577, Japan. Tel.: +81 3 5315 9357.

E-mail address: dbridges50@gmail.com (R. Hashimoto).

used to quantify different aspects of water diffusion within a tissue (i.e., anisotropy, magnitude, and type of anisotropy). Previous DTI studies have demonstrated that individuals with ASD show atypical fractional anisotropy (FA) values in several major WM tracts, including the bilateral inferior longitudinal fasciculi, bilateral inferior fronto-occipital fasciculi, bilateral uncinate fasciculi, and bilateral corticospinal tracts (Bakhtiari et al., 2012; Barnea-Goraly et al., 2010; Billeci et al., 2012; Gibbard et al., 2013; Jou et al., 2011; Kleinhans et al., 2012; Weinstein et al., 2011), many of which are accompanied with alterations in mean diffusivity (MD) (e.g., Kleinhans et al., 2012). FA is a commonly used metric that represents the degree of anisotropy of water diffusion, while MD quantifies the magnitude of water diffusion. In addition, Ennis and Kindlmann (2006) have recently introduced a new metric named mode of tensor (MO), which specifies the type of anisotropy, ranging from planar to linear. Although no studies to date have examined possible alterations in MO of ASD, its applicability has been demonstrated in a recent study of mild cognitive impairment in which abnormalities had been detected only in MO but not in FA (Douaud et al., 2011). Therefore, analysis of MO may further reveal previously undetected WM abnormalities in the ASD brain.

While single modality analyses of VBM and DTI have already generated many findings on structural alterations in the ASD brain, the interrelated associations between these alterations are poorly understood. Visual inspection of patterns of GM and WM alterations may be suggestive of some common pathological changes affecting brain regions and their connecting pathways such as the network involved in cognitive and affective functions, including the ventrolateral amygdala, lateral orbitofrontal cortex, and fusiform gyrus. In an effort to investigate such possibilities, several recent studies have adopted a new approach in which multimodal brain imaging data are collected from the same subject. Indeed, multimodal brain imaging is increasingly playing important roles in revealing structural–structural (i.e., gray and white matters) or structural–functional associations in normal (Ethofer et al., 2011; Li et al., 2013) and clinical populations, including Alzheimer's disease (Jacobs et al., 2012), schizophrenia (Schlosser et al., 2007), autism (Beacher et al., 2012; Mengotti et al., 2011), and other diseases (Ambrosi et al., 2013; Haller et al., 2013; Quinque et al., 2012; Ruef et al., 2012). For instance, Kana et al. (2014) acquired functional MRI (fMRI) data during a social cognition task and DTI data from each individual with ASD and normal control; the multimodal data were analyzed separately, and then combined together only when interpreting resultant statistical maps. Although such approaches can surely advance our understanding of relationships between different aspects of abnormalities in the ASD brain, it has limitations in its detectability and interpretability since different modalities are integrated after separate statistical analyses. Therefore, new mathematically grounded methods of fusing different imaging modalities will be needed to obtain a more comprehensive view for the neuroanatomical underpinnings in the ASD brain.

Several new methods have been proposed in order to fuse multimodal data in a data-driven way (Sui et al., 2012, 2013c). Moreover, these new methods have been applied to several combinations of modalities such as DTI and fMRI (e.g., Franco et al., 2008; Groves et al., 2012; Mangalathu-Arumana et al., 2012; Sui et al., 2011, 2013b; Teipel et al., 2010). For instance, linked independent component analysis (ICA) is a recently developed, multimodal data-fusion method proposed by Groves et al. (2011), which decomposes multimodal dataset into a set of statistically independent components linked in terms of a shared loading matrix, each column of which represents subject-course (or component loading) *shared* across modalities. Furthermore, previous studies have suggested that experience-driven plasticity or neurotrophic effects might induce co-variation between cortical regions and their relevant WM pathways (Lerch et al., 2006; Pascual-Leone et al., 2005; Pezawas et al., 2004). Considering these findings, the present study examined the possibility that linked ICA can be used to detect co-occurring

alterations in GM and WM that underlie various clinical manifestations in ASD.

The present study aimed to uncover co-occurring alterations in GM morphology and WM microstructure of the ASD brain using linked ICA. Given numerous VBM and DTI studies indicating abnormalities in GM regions and WM tracts, we expected that our linked ICA analysis would identify patterns of atypical shared loadings in some composite components. Furthermore, we expected that such GM and WM abnormalities would be largely found in areas responsible for impaired cognitive and affective functions in ASD, possibly regions related to core clinical problems such as social cognition and interaction.

2. Materials and methods

2.1. Participants

Forty-six adult males with ASD were recruited from outpatient units of the Karasuyama Hospital, Tokyo, Japan. All patients were assessed by a team of three experienced psychiatrists and a clinical psychologist, and then were diagnosed with ASD, based on the criteria of the Diagnostic and Statistical Manual of Mental Disorders, Fourth Edition (DSM-IV) and a medical chart review. The assessment consisted of participant interviews about developmental history, present illness, life history, and family history assessed independently by a psychiatrist and a clinical psychologist in the team. Patients were also asked to bring suitable informants who had known them in early childhood. At the end of the interviews, the patients were formally diagnosed with a pervasive developmental disorder by the psychiatrist if there was a consensus between the psychiatrists and the clinical psychologist; this process required approximately 3 h. A pair of psychiatrists and the clinical psychologist also confirmed that none of the patients met the DSM-IV criteria for any other psychiatric disorder. A total of 46 age-matched normal male controls (NCs) were recruited by advertisements and acquaintances. None of the NCs reported any severe medical problem, or any neurological or psychiatric history. None of them satisfied the diagnostic criteria for any psychiatric disorder. The intelligence quotient (IQ) scores of all participants with ASD were evaluated using either the Wechsler Adult Intelligence Scale—Third Edition (WAIS-III) or the WAIS—Revised (WAIS-R), while those of NCs were estimated using a Japanese version of the National Adult Reading Test (JART) (Matsuoka et al., 2006). Every participant with ASD was considered to be high functioning since their full-scale IQ scores were higher than 80. Handedness was assessed using the Edinburgh Handedness Inventory (Oldfield, 1971). Participants completed the Japanese version of the Autism-Spectrum Quotient (AQ) test (Wakabayashi et al., 2006).

Table 1 showed the demographic and clinical data of participants in both the ASD and NC groups. Age and IQ were matched between the two groups (all $p > 0.15$). The Edinburgh handedness score of the NC group was significantly higher than that of the ASD group ($p = 0.01$). At the time of the MRI scans, 14 of the 46 participants with ASD were using one or more of the following medications: anti-depressants (9 patients), hypnotic drugs (9 patients), anti-anxiety drugs (7 patients), anti-epileptic drugs (4 patients), and anti-psychotic drugs (4 patients). Thirteen of the 46 participants with ASD received cognitive behavioral therapy (CBT) and/or social skills training (SST) at the day-care center of Karasuyama Hospital. None of the participants attended the therapy or training sessions longer than 12 h per week (on average 3 h per week). In this study, one or both of the Autism Diagnostic Observation Schedule (ADOS) Module 4 (Lord et al., 2000) and/or the Diagnostic Interview for Social and Communicative Disorders (DISCO), a structured and validated interview procedure for the diagnosis of autism (Maljaars et al., 2012; Wing et al., 2002), were administered to 28 of the 46 participants with ASD by trained and experienced psychiatrists. Nine subjects were confirmed to satisfy the diagnostic criteria for ASD by the DISCO, while 9 subjects were confirmed to satisfy the diagnostic

Table 1
The demographic data for the participants.

	NC (n = 46)			ASD (n = 46)			Statistics	
	Mean	SD	Range	Mean	SD	Range	df	p-Value
Age (years)	30.54	6.39	19–47	30.21	7.48	19–50	90	0.82
Full-scale IQ	109.22	7.47	95.5–119.8	106	14.22	82–134	90	0.18
Handedness	90.88	23.17	5.3–100	61.88	68.02	−100–100	86	0.01
AQ score	15.42	6.04	3–30	35.90	4.90	24–47	80	<0.001
ADOS								
Total				13.26	3.75	5–20		
Communication				4.7	2.02	2–9		
Social reciprocity				8.53	2.22	3–11		

Note: WAIS-III or -R was administered to all participants with ASD, and the IQ score was estimated for all NCs based on JART.
The AQ score was collected from 36 NCs and all participants with ASD.

criteria for ASD by the ADOS; the remaining 10 subjects were confirmed by both the DISCO and ADOS. In two subject, the total ADOS scores were lower than the cut-off score (<7); however, one of these subjects satisfied the cut-off scores for the "communication" and "social reciprocity" subscales of ADOS, while the other subject satisfied the cut-off score for the "communication" subscale of ADOS with the DISCO further confirming the diagnosis of ASD in this subject; therefore, we regarded these two participants as being part of the ASD group in this study.

2.2. MRI data acquisition

All MRI data were acquired using a 1.5 Tesla GE, Signa system (General Electric, Milwaukee, WI, USA) with a phased-array whole-head coil. Diffusion-weighted images were acquired using an echo-planar imaging (EPI) acquisition sequence with one $b0$ image and 30 directions of diffusion gradients (in-plane resolution: 1.875×1.875 mm, 3 mm slice thickness with no gap, repetition time (TR): 12 s, echo time (TE): 78.9 ms, flip angle: 90°, b-value = 1000 s/mm, matrix size: 128×128, 50 axial slices, number of excitation = 2). In addition, a high-resolution T1-weighted spoiled gradient recalled (SPGR) 3D MRI image was collected (in-plane resolution: 0.9375×0.9375 mm, 1.4 mm slice thickness, TR: 25 ms, TE: 9.2 ms, matrix size: 256×256, 128 sagittal slices).

2.3. Data preprocessing

2.3.1. DTI data preprocessing and statistics using TBSS

All diffusion-weighted images were preprocessed using the FMRIB's Diffusion Toolbox (FDT) software, which is a part of the FMRIB's Software Library (FSL) version 5. 0. 0 (Smith et al., 2004). First, raw data were visually inspected and were discarded when any artifacts, including large intensity differences in any of the slices and checkers, were observed in any volume; eddy current correction was then performed for each participant. Then, the motion-corrected data were further visually inspected to detect any artifacts or registration errors; no participant in this study was excluded due to excessive artifact-contaminated volumes (>10 removed volumes) (Jones, 2004; Papadakis et al., 2000). To confirm whether or not our visual inspection was able to detect volumes with artifacts, the quality of the data was further assessed using the DTIPrep software (Oguz et al., 2014). We found that no additional disrupted volumes were detected. After removing the corrupted volumes, the gradient files (i.e., bval and bvec files) were modified to reflect these changes. Then, the tensor model was used to obtain semi-quantitative scalar measures, such as FA, MD, and MO. Finally, we visually inspected the FA map obtained by the aforementioned procedure for additional distortions (e.g., red-colored or blurred FA maps). None of the participant in this study showed such abnormal FA patterns.

A total of 92 FA maps obtained by the aforementioned procedures were further preprocessed with a standard protocol of tract-based spatial statistics (TBSS; Smith et al., 2006). First, all FA images were aligned to a common space using the nonlinear registration tool FNIRT, which uses a b-spline representation of the registration warp field (Andersson et al., 2007). A mean FA image and mean FA skeleton, representing the centers of all tracts common to all participants, were then created. FA values of individual voxels were projected onto the mean FA skeleton for each participant. For subsequent analyses, MD and MO maps were also projected onto the mean FA skeleton using the affine and non-linear transformations applied to FA maps.

For between-group comparison, a permutation-based nonparametric testing with 5000 permutations was independently performed on skeletonized FA, MD, and MO maps. Results were corrected for multiple comparisons using threshold-free cluster enhancement (TFCE) implemented in FSL (Smith and Nichols, 2009). Of note, age was included as a nuisance covariate. Significance level was set to $p < 0.05$. If any significant between-group differences were detected, associations between DTI measures and autism scales (AQ and ADOS scores) were investigated for voxels showing significant alterations, while including age as a controlling variable.

2.3.2. T1-weighted image preprocessing and statistics using VBM

All T1-weighted images were preprocessed using FSL-VBM (Douaud et al., 2007; http://fsl.fmrib.ox.ac.uk/fsl/fslwiki/FSLVBM/), an optimized VBM protocol (Good et al., 2001) carried out with FSL tools. First, each T1-weighted image was brain-extracted using the Brain Extraction Tool (BET), and then tissue-type segmentation was performed using FAST (Zhang et al., 2001). Next, the resulting images were aligned to the Montreal Neurological Institute (MNI) 152 standard space. The aligned images were averaged to create a study-specific template, to which native GM images were then non-linearly registered using FNIRT. The registered partial volume images were then modulated to correct for local expansion or contraction by dividing the Jacobian of the warp field. Finally, the modulated segmented images were spatially smoothed using an isotropic Gaussian kernel with a sigma of 4 mm (FWHM = 9.4 mm).

As was the case with TBSS analysis, a permutation-based non-parametric testing with 5000 permutations was performed on the smoothed, modulated, and segmented GM volumes for between-group comparison. The result was corrected for multiple comparisons using TFCE (Smith and Nichols, 2009). Of note, age and total brain volume (TBV) (described below) were included as nuisance covariates. If any significant between-group differences were detected, associations between GM volume and autism scales (AQ and ADOS scores) were investigated for voxels showing significant alterations, while including age as a controlling variable.

In addition, for each participant, brain tissue volumes normalized for head size were estimated with SIENAX (Smith et al., 2002). Briefly, brain and skull images were first extracted from the original T1-weighted images; then, brain images were affine-registered to the MNI 152 standard space (Jenkinson et al., 2002; Jenkinson and Smith, 2001). Finally, tissue-type segmentation with partial volume estimation was carried out in order to calculate the total volume of brain tissue (Zhang et al., 2001).

2.4. Linked ICA

Linked ICA was performed to investigate the associations between GM morphology and WM structure in terms of shared component loadings. In this study, a VBM measure (GM volume) and three DTI measures (FA, MD, and MO) were fed into the linked ICA algorithm as a set of inputs based on a previous study (Groves et al., 2011). Since MO is mathematically orthogonal to FA and MD, inclusion of this metric might have facilitated evaluation of associations between the two different aspects in the ASD brain. The linked ICA method has been described in details elsewhere (Groves et al., 2011, 2012). Briefly, this method is a data-driven approach for fusing multimodal data. This approach decomposes the given data into a set of statistically independent components and a loading matrix shared across modalities, each column of which indicates the degree of contribution of the corresponding component for each participant. Although linked ICA originally proposed with a tensor (multidimensional array) model configuration, the present study used a flat model configuration that required no assumption about the spatial alignment among DTI measures of FA, MD, and MO. Of note, all input data were down-sampled for computational efficiency (DTI data: $2 \times 2 \times 2$ mm^3, GM: $4 \times 4 \times 4$ mm^3), using the procedure employed by a previous study (Groves et al., 2012). In this study, the spatial smoothness (i.e., the degree of freedom per voxel) of each modality was estimated based on the eigenspectrum of the data (Beckmann and Smith, 2004). The degrees of freedom per voxel were estimated as 0.019 for FA, 0.015 for MD, 0.026 for MO, and 0.007 for GM. The number of independent components was set to 90, because a high-dimensional model can segregate meaningful components from artifactual components, as has been demonstrated by previous studies (Groves et al., 2011, 2012).

Statistical analysis for the group comparison was performed using a general linear model implemented in the Statistics toolbox for MATLAB (R2012a; MathWorks). The main effect of group (G_i) for each column of the shared loading matrix, **H**, obtained by the linked ICA was estimated by fitting a general linear model with age and total brain volume as covariates as follows:

$$h_{ij} = \beta_0 + \beta_1 G_i + \beta_2 Age_i + \beta_3 TBV_i + \varepsilon_{ij},$$

where ε_{ij} is the residual error of the (i,j)-th element of the shared loading matrix. For each column of the shared loading matrix, between-group difference was estimated from β_1 normalized by the corresponding standard error, and a false discovery rate (FDR) correction was used for multiple comparisons (Storey, 2002). If any significant between-group differences were found, associations between the altered component loadings and other variables (age, TBV, AQ, and ADOS scores) were further investigated using correlation analyses.

It should be noted that the signs (positive or negative) of the component loadings and the corresponding components were essentially ambiguous due to the sign indeterminacy of ICA (Comon and Jutten, 2010). Therefore, one needs to take into account the combination of the signs of the z-stats of the component maps and those of the component loadings to correctly interpret the results of the linked ICA regarding the direction of alteration (i.e., reductions or increases) in one group with reference to the other. For example, voxels with positive z-stats will be regarded as being increases in VBM and DTI metrics for the NC group (i.e., NC > ASD) if the mean component loading of the ASD group is *smaller* than that of the NC group (Supplementary Fig. 1A). On the other hand, voxels with negative z-stats will also be regarded as being increases in the metrics for the NC group (i.e., NC > ASD) if the mean component loading of the ASD group is greater than that of the NC group (Supplementary Fig. 1B). For simple illustrative examples exhausting all possible cases, see Supplementary Fig. 1.

2.5. Probabilistic tractography

It turned out that two of the 90 composite components showed significant between-group differences (see Results). In one of the components (component #13), we observed widespread GM alterations involving multiple brain regions critically implicated in the pathophysiology of ASD, such as the bilateral fusiform gyri, bilateral orbitofrontal cortices, and bilateral motor cortices. To elaborate the relationship between the spatial patterns in the GM and WM maps of that component, we delineated anatomical connections between some of the major clusters in the GM map using probabilistic tractography (Behrens et al., 2007). Among the many pairs of brain regions identified in the GM map of component #13, we reasoned that clear relationships with WM maps could be shown at least for the following three connections by tractography: (1) connection between the right fusiform gyrus and right anterior temporal pole, because these regions have been implicated in face perception (Cohen Kadosh and Johnson, 2007) and are anatomically connected via the right inferior longitudinal fasciculus; (2) connection between the right anterior temporal pole and right orbitofrontal cortex, because these regions have been implicated in the integration of emotion with cognitive behavior (Catani et al., 2013) and are connected via the right uncinate fasciculus; and (3) connection between the left putamen and left pre- and post-central gyri, because these regions are involved in motor control (Stoodley et al., 2012) and are connected via the left corticospinal tract. Note that these three functions are significantly impaired in ASD and that these tracts have been reliably reconstructed in previous DTI tractography studies (e.g., Catani and Thiebaut de Schotten, 2008). Because the original GM map obtained by the linked ICA included large voxel clusters extending into multiple brain regions, the map was thresholded to yield distinct clusters for seed and target regions with moderate sizes ($z < -6.0$ for the right anterior temporal pole; $z < -2.3$ for the left putamen; $z > 2.3$ for the right orbitofrontal cortex; $z > 6.0$ for the right fusiform gyrus and left pre- and post-central gyri). The MNI coordinates and the number of voxels of seed and target regions are listed in Table 2.

For each participant, probabilistic tractography was performed from all voxels in each seed mask using probtrackx2 implemented in FSL (Behrens et al., 2007). In order to discard streamlines that crossed to the contralateral hemisphere, an exclusion mask was generated on the standard space (MNI coordinate: $x = 0$). For each participant, a seed, target, and exclusion masks defined on the standard space were then transformed into a native DTI space. For each voxel within the seed mask, 5000 streamlines were sampled with a step length of 0.5 mm and a curvature threshold of 0.2. The streamlines were terminated when they reached to the target mask. Streamlines that did not pass or reach to the target mask within 2000 steps were discarded. By adding the exclusion mask, streamlines that crossed to the contralateral hemisphere were also discarded.

To visualize the spatial distribution of the connection between each pair of seed and target regions, we created a tract representing the spatial overlap of the streamlines across all participants. For each participant, a tract obtained by probabilistic tractography was divided by the total number of successful streamlines and binarized by setting voxels having greater than 0.01 to 1 and the remaining voxels to 0. The

Table 2
The MNI coordinates and cluster sizes of seed and target masks used for probabilistic tractography.

Brain region	MNI coordinate (center of gravity)			Size
	x	y	z	
Right fusiform gyrus	34.3	−59	−17.4	873
Right anterior temporal pole	54.3	5.4	−19.3	535
Right orbitofrontal cortex	22.7	35.1	−17.4	645
Left putamen	−25.3	9.8	−0.2	244
Left pre- and post-central gyri	−44.6	−21.7	50	2703

binarized tract was transformed from a native DTI space into the standard space. The binarized tracts in the standard space were then summed across all participants and divided by the total number of participants ($n = 92$). We further binarized the normalized tract by setting voxels having greater than 0.1 to 1 and the remaining voxels to 0, to reconstruct a representative tract. Finally, we examined the spatial overlap between each reconstructed WM tract and the voxels in the FA map of component #13 by overlaying the two in a single figure.

3. Results

3.1. Results of VBM and TBSS analyses

VBM analysis on GM revealed no clusters of voxels that showed between-group difference beyond the significance level. In contrast, TBSS analysis revealed that widely distributed patterns of alterations in FA and MD values, but not in MO values, in participants with ASD when compared to NCs (Fig. 1). More specifically, participants with ASD showed significant FA reductions in projection fibers (the bilateral corticospinal tracts and bilateral anterior thalamic radiations), commissural fibers (the body and splenium of the corpus callosum), and association fibers (the left uncinate fasciculus, bilateral inferior and superior

longitudinal fasciculi, and bilateral inferior fronto-occipital fasciculi) (see Table 3 and Fig. 1A). On the other hand, a significantly increased MD for ASD was found in projection fibers (the bilateral corticospinal tracts and bilateral anterior thalamic radiations), commissural fibers (the body and splenium of the corpus callosum), and association fibers (the bilateral uncinate fasciculi, bilateral inferior and superior longitudinal fasciculi, bilateral inferior fronto-occipital fasciculi, and left cingulum) (see Table 4 and Fig. 1B). Notably, alterations in FA and MD were substantially overlapped in several tracts (e.g., the right inferior longitudinal fasciculus: 597 voxels; right inferior fronto-occipital fasciculus: 675 voxels) (see Supplementary Table 1, for other tracts). None of the autism scales (AQ and ADOS scores) were significantly associated with either FA or MD.

3.2. Results of linked ICA

Linked ICA decomposed the multimodal data into 90 independent components and a shared loading matrix. Statistical analysis on the loading matrix detected significant between-group differences in two components (#1: $t = 2.256$, $p = 0.027$; #13: $t = 3.566$, $p < 0.001$, uncorrected), one of which passed the FDR corrections for multiple comparisons (#13: $p = 0.047$, FDR-corrected) (Fig. 2A and C). For both components, DTI metrics, especially FA and MO, dominantly
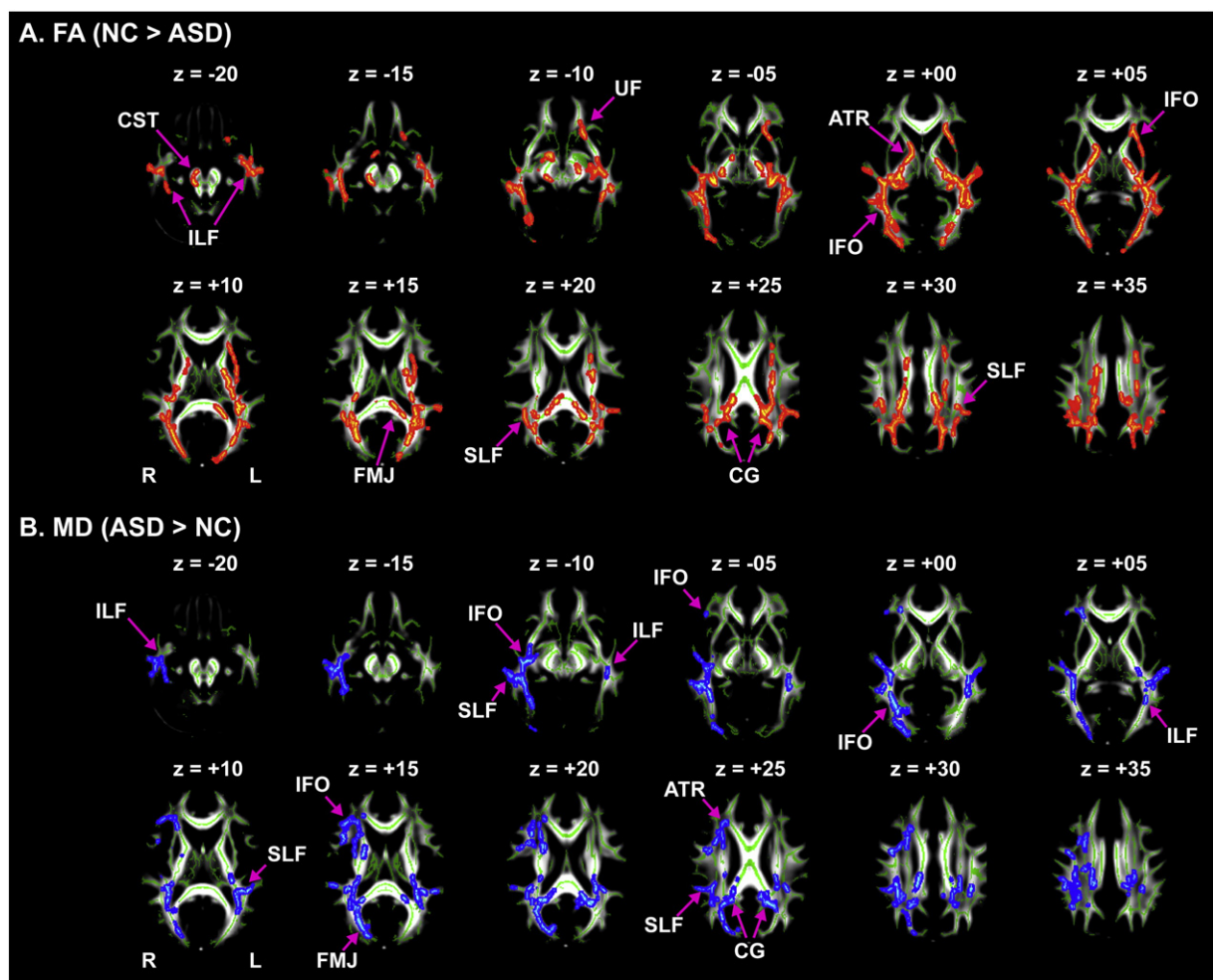

Fig. 1. Decreased fractional anisotropy and increased mean diffusivity in participants with autism spectrum disorder compared to normal controls. TBSS analysis revealed that participants with autism spectrum disorder (ASD) showed widespread fractional anisotropy (FA) reductions in major white matter tracts (A), while they showed increased mean diffusivity (MD) in similar white matter tracts (B). For each statistical analysis, significance level was set at $p < 0.05$, TFCE-corrected. For visualization purpose, significant regions were thickened using *tbss_fill*. R: Right, L: left, ART: anterior thalamic radiation, CG: cingulum, CST: corticospinal tract, FMJ: forceps major, IFO: inferior fronto-occipital fasciculus, IFL: inferior longitudinal fasciculus, SLF: superior longitudinal fasciculus, and UF: uncinate fasciculus.

Table 3
Decreased fractional anisotropy in participants with autism spectrum disorder compared to normal controls.

Cluster	Size	MNI coordinate (Center of gravity)				Tract label	Hemisphere
		x	y	z	p-Value		
#1	9305	−28.4	−32.5	14.6	0.019	Inferior fronto-occipital fasciculus	L
						Anterior thalamic radiation	L, R
						Corticospinal tract	L
						Cingulum (cingulate gyrus)	L
						Cingulum (hippocampus)	L
						Inferior longitudinal fasciculus	L
						Superior longitudinal fasciculus	L, R
						Uncinate fasciculus	L
						Superior longitudinal fasciculus (temporal part)	L, R
#2	7530	29.7	−41.3	12.5	0.026	Inferior fronto-occipital fasciculus	R
						Anterior thalamic radiation	L, R
						Corticospinal tract	L, R
						Cingulum (cingulate gyrus)	R
						Cingulum (hippocampus)	L, R
						Forceps major	I
						Inferior longitudinal fasciculus	R
						Superior longitudinal fasciculus	R
						Superior longitudinal fasciculus (temporal part)	R
#3	628	18.1	−12.3	46.7	0.043	Corticospinal tract	R
						Anterior thalamic radiation	R
						Cingulum (cingulate gyrus)	R
						Superior longitudinal fasciculus	R
						Superior longitudinal fasciculus (temporal part)	R
#4	11	25.5	−15.1	−8.09	0.05	Inferior fronto-occipital fasciculus	R
						Inferior longitudinal fasciculus	R

Note: R: right, L: left, I: inter-hemispheric. White matter tracts altered in participants with autism spectrum disorder were labeled in accordance with the John's Hopkins University (JHU) atlas.

contributed to the construction of the altered component loadings (FA: 62%, MD: 18%, MO: 18%, and GM: 2% for #1; FA: 34%, MD: 6%, MO: 52%, and GM: 8% for #13) (Fig. 2B and D).

Loading of component #1 (Fig. 3) showed a between-group difference and partial correlation analyses revealed significant associations with age (combined: $r = -0.300$, $p = 0.004$, NC: $r = -0.320$, $p = -0.032$; ASD: $r = -0.279$, $p = 0.063$, uncorrected) while adding TBV as a controlling variable. This component showed global FA reductions along with globally increased MD in participants with ASD (Fig. 3A and B). On the other hand, MO showed changes, including

Table 4
Increased mean diffusivity in participants with autism spectrum disorder compared to normal controls.

Cluster	Size	MNI coordinate (center of gravity)				Tract label	Hemisphere
		x	y	z	p-Value		
#1	7439	33.4	−35.8	17.8	0.034	Inferior longitudinal fasciculus	R
						Anterior thalamic radiation	L, R
						Corticospinal tract	R
						Cingulum (cingulate gyrus)	R
						Cingulum (hippocampus)	R
						Forceps major	I
						Inferior fronto-occipital fasciculus	R
						Superior longitudinal fasciculus	R
						Uncinate fasciculus	R
						Superior longitudinal fasciculus (temporal part)	R
#2	2155	−29.8	−40	19.2	0.038	Anterior thalamic radiation	L, R
						Corticospinal tract	L
						Cingulum (cingulate gyrus)	L
						Cingulum (hippocampus)	L
						Forceps major	I
						Inferior fronto-occipital fasciculus	L
						Superior longitudinal fasciculus	L, R
						Uncinate fasciculus	L
						Superior longitudinal fasciculus (temporal part)	L, R
#3	1174	29.7	19.7	18.6	0.043	Superior longitudinal fasciculus	R
						Anterior thalamic radiation	R
						Corticospinal tract	L, R
						Cingulum (cingulate gyrus)	R
						Forceps minor	I
						Inferior fronto-occipital fasciculus	R
						Uncinate fasciculus	R
						Superior longitudinal fasciculus (temporal part)	R

Note: R: right, L: left, I: inter-hemispheric. White matter tracts altered in participants with autism spectrum disorder were labeled in accordance with the John's Hopkins University (JHU) atlas.
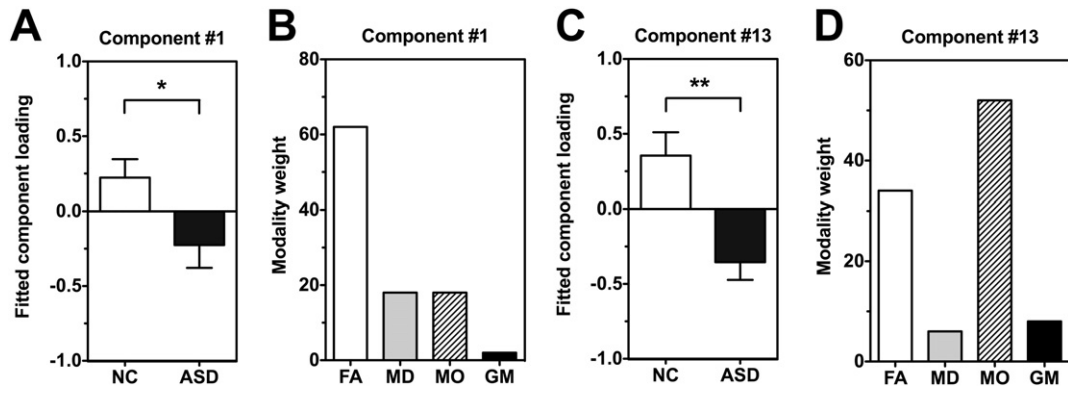
Fig. 2. Altered component loadings of two components and contributions of each modality to these altered variation profiles. (A) Altered fitted loading of component #1. In this component, the group of autism spectrum disorder (ASD) exhibited significant decreases in component loading compared to the group of normal controls (NCs) (NC: 0.223 ± 0.123 (mean ± standard error of the mean); ASD: −0.225 ± 0.153; $p = 0.027$, uncorrected). (B) The contributions of four modalities to loading of the first component. Fractional anisotropy (FA) dominantly contributed to the construction of this component loading (62%), while the contributions of mean diffusivity (MD), mode of tensor (MO), and gray matter (GM) were 18%, 18%, and 2%, respectively. (C) Altered fitted loading of component #13. In this component, the ASD group exhibited significant decreases in component loading compared to the NC group (NC: 0.354 ± 0.156; ASD: −0.354 ± 0.119; $p < 0.001$, uncorrected). Of note, loading of this component passed a correction for multiple comparisons ($p = 0.047$, FDR-corrected). (D) The contributions of four modalities to loading of the component #13. FA and MO dominantly contributed to the construction of this component loading (34% and 52%, respectively), while the contributions of MD and GM were 6% and 8%, respectively. *: $p < 0.05$, uncorrected; **: $p < 0.001$, uncorrected.
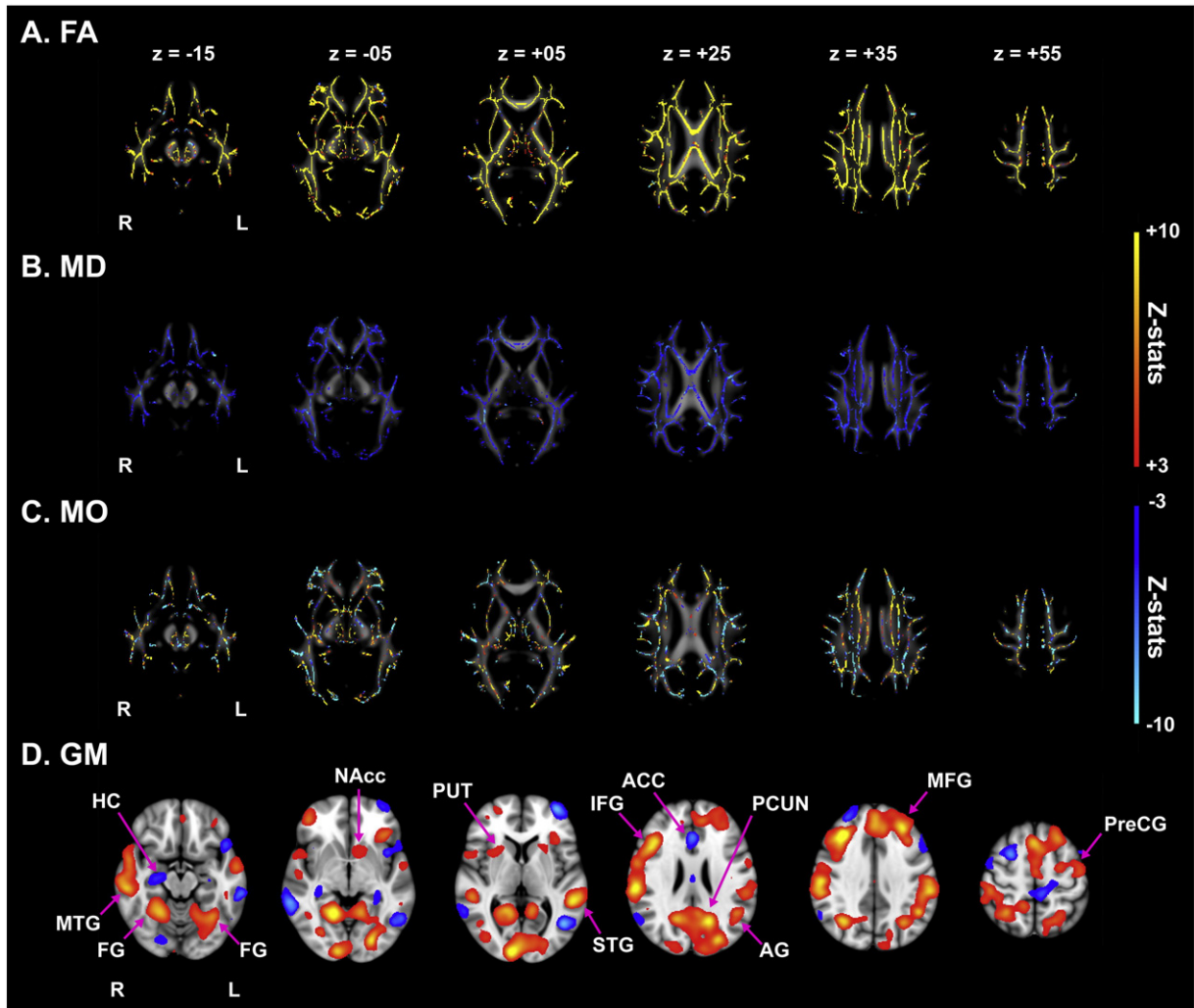

Fig. 3. Visualization of component #1 for fractional anisotropy, mean diffusivity, the mode of tensor, and gray matter, respectively. This component shows global increases in fractional anisotropy (FA; A) and global decreases in mean diffusivity (MD; B). The mode of tensor (MO; C) can be generally visualized as increasing, while gray matter (GM; D) can be seen as comprising of several cortical and sub-cortical regions, such as the left superior temporal gyrus (STG) and bilateral putamen (PUT). The red-yellow color stands for positive z-stats, while the light-blue color indicates negative z-stats. R: Right, L: left, ACC: anterior cingulate cortex, AG: angular gyrus, FG: fusiform gyrus, HC: hippocampus, IFG: inferior frontal gyrus, MFG: middle frontal gyrus, MTG: middle temporal gyrus, NAcc: nucleus accumbens, PCUN: precuneus, and PreCG: precentral gyrus.
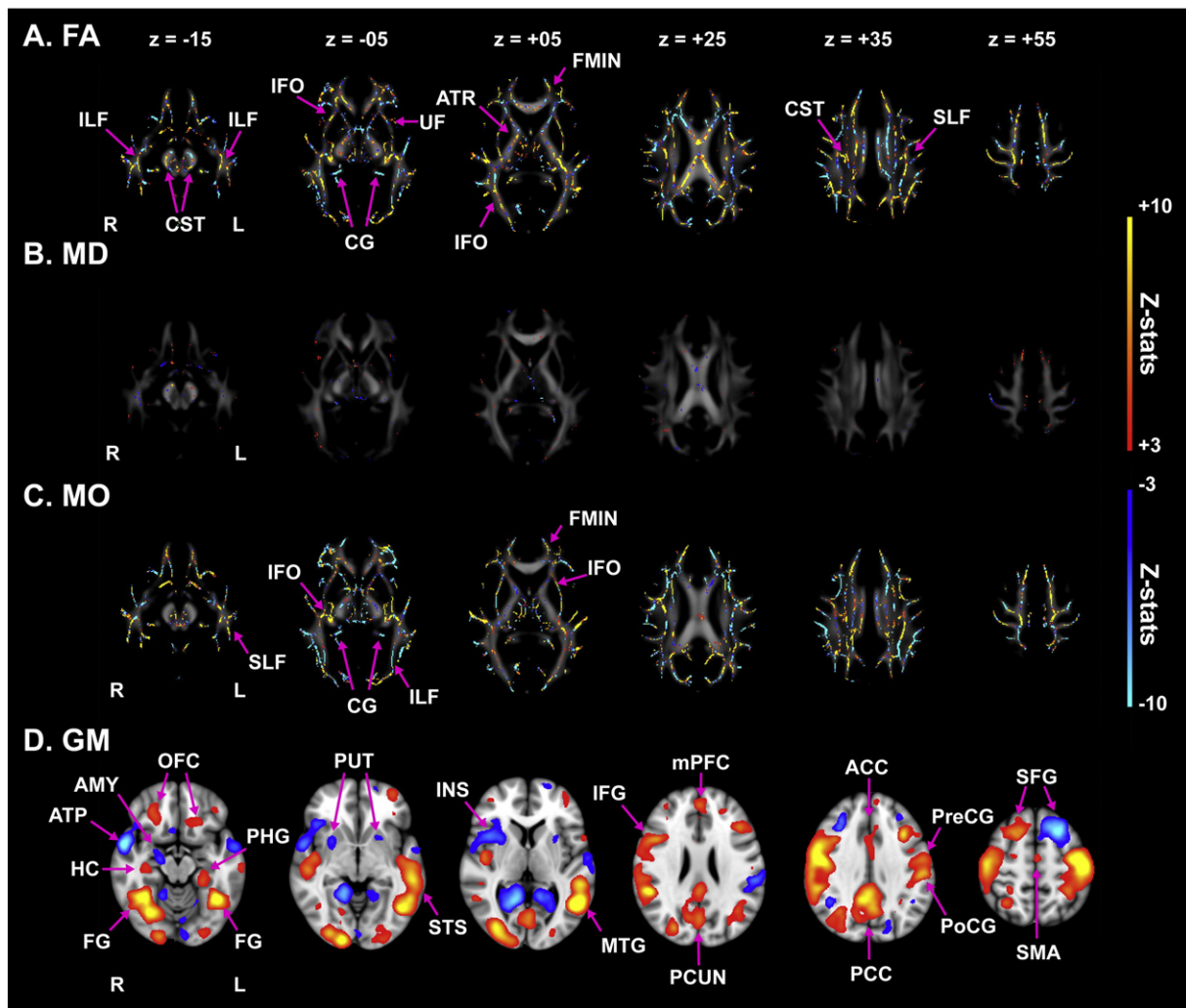
Fig. 4. Visualization of component #13 for fractional anisotropy, mean diffusivity, the mode of tensor, and gray matter. Component #13 showed increases in fractional anisotropy (FA; A) in several major white matter tracts, such as the bilateral inferior fronto-occipital fasciculi (IFOs) and corticospinal tracts (CSTs). The mean diffusivity (MD; B) showed small local changes. The mode of tensor (MO; C) co-varied with the pattern of FA. The gray matter (GM; D) comprised several cortical and sub-cortical regions, such as the bilateral fusiform gyri (FGs) and pre- and post-central gyri (PreCGs and PoCGs). The red-yellow color stands for positive z-stats, while the light-blue color indicates negative z-stats. R: Right, L: left, ATR: anterior thalamic radiation, CG: cingulum, F$_{min.}$: forceps minor, IFL: inferior longitudinal fasciculus, SLF: superior longitudinal fasciculus, UF: uncinate fasciculus, ACC: anterior cingulate cortex, Amy: amygdala, ATP: anterior temporal pole, HC: hippocampus, IFG: inferior frontal gyrus, INS: insula, mPFC: medial prefrontal cortex, MTG: middle temporal gyrus, OFC: orbitofrontal cortex, PCC: posterior cingulate cortex, PCUN: precuneus, PHG: parahippocampal gyrus, SFG: superior frontal gyrus, SMA: supplementary motor area, and STS: superior temporal sulcus.

bilateral increases in the superior longitudinal fasciculi, and bilateral decreases in the thalamus in ASD (Fig. 3C). GM was generally seen to be decreasing in the left superior temporal gyrus, bilateral putamen, left nucleus accumbens, and right inferior frontal gyrus in participants with ASD compared to NCs (Fig. 3D).

Loading of component #13 showed a significant between-group difference, while showing no significant correlations with other variables (all $p > 0.25$). Compared to NCs, participants with ASD exhibited FA reductions mainly in the bilateral corticospinal tracts, bilateral inferior longitudinal fasciculi, bilateral inferior fronto-occipital fasciculi, and bilateral uncinate fasciculi (Fig. 4A); notably, the pattern of FA reduction in this component substantially overlapped with that of the decreased FA revealed by TBSS analysis (e.g., the right inferior longitudinal fasciculus: 631 voxels) (see Supplementary Table 2, for other tracts). On the other hand, MD showed small local changes (Fig. 4B), which partially overlapped with the locally increased MD in ASD (e.g., the forceps major) shown by TBSS analysis. The spatial pattern of MO was highly similar to that of FA (Fig. 4C). In this component, participants with ASD showed decreased GM volumes mainly in the bilateral fusiform gyri, bilateral orbitofrontal cortices, medial prefrontal cortex, posterior cingulate cortex, right hippocampus, and bilateral pre- and

post-central gyri and increased volumes mainly in the bilateral anterior temporal poles, bilateral lingual gyri, bilateral putamen, and right amygdala (Fig. 4D).

Linked ICA modeled the *shared* subject-course (component loading) from a multimodal data; however, it is possible to regenerate the subject-courses of all components in each modality. Following the procedures described by Groves et al. (2012), we regenerated each modality's subject-course of component #13, in order to confirm that all of the modalities, rather than just a few modalities, showed atypical subject-courses in this component. Although the modality weights of GM and MD were relatively smaller than those of FA and MO, partial correlation analyses revealed that subject-courses of all the modalities were significantly correlated with diagnosis (FA: $r = 0.359$, $p < 0.001$; MD: $r = 0.350$, $p < 0.001$; MO: $r = 0.350$, $p < 0.001$; GM: $r = 0.351$, $p < 0.001$; all: $r = 0.357$, $p < 0.001$). Although each modality's subject-course of component #13 exhibited a significant between-group difference, this does not indicate directly that participants with ASD showed significant alterations in all modalities. In particular, we need to be cautious in interpreting the results of some modalities that had weak contribution to the construction of the shared subject-course, because the linked ICA tends to match the subject-courses of weakly contributed

modalities (e.g., GM) to those of strongly contributed modalities (e.g., FA and MO). Although the contribution of GM to the shared subject-course was substantially weaker than that of other modalities, such as FA and MO, the GM map comprised several brain regions linked with the neuropathology of ASD (e.g., the bilateral fusiform gyri). In addition, the probabilistic tractography demonstrated that the connections between brain regions observed in the GM map were altered (see next section). These results suggest that even weakly contributed modalities, at least GM, might be altered in the ASD brain.

3.3. Visualization of reconstructed WM tracts using probabilistic tractography

In order to confirm whether alterations in the GM and WM maps of this component were indeed linked, we performed probabilistic tractography to reconstruct three connections between major loci of GM alterations (Fig. 4D): (1) connection between the right fusiform gyrus and right anterior temporal pole; (2) connection between the right anterior temporal pole and right orbitofrontal cortex; and (3) connection between the left putamen and left pre- and post-central gyri (see Methods). We observed spatial overlaps between reconstructed tracts and voxels in the FA map of the linked ICA (Fig. 5), indicating the possibility of co-occurred morphological alterations in the ASD brain.

4. Discussion

This study examined alterations in the neuroanatomy of participants with ASD using two different modalities: structural MRI and DTI. Specifically, in addition to conventional separate unimodal analyses (VBM and TBSS), we aimed to investigate co-occurring alterations in both GM and WM morphology. In order to do this, we employed linked ICA (Groves

Fig. 5. Visualization of reconstructed WM tracts connecting the brain regions identified in the GM map of component #13. Using probabilistic tractography, the following three connections were delineated: (A) connection between the right fusiform gyrus (FG) and right anterior temporal pole (ATP); (B) connection between the right ATP and right orbitofrontal cortex (OFC); and (C) connection between the left putamen (PUT) and left pre- and post-central gyri (Pre/PostCG) identified in the GM map of component #13 (Fig. 4D). The fractional anisotropy (FA) map of component #13 was overlaid to examine whether voxels of the FA map were overlapped with the reconstructed tracts. For visualization purpose, we adopted the extent threshold (>40 voxels) and z-stats threshold ($|z| > 2.3$) to the FA map. Voxels with positive z-stats (>2.3) were represented as the red-yellow color, while voxels with negative z-stats (<−2.3) were represented as the light-blue color.

et al., 2011), which is a data-driven multimodal analysis. Unimodal analyses revealed that, although between-group differences in GM volume did not reach significance, participants with ASD showed widespread FA reductions, accompanied by increased MD, in major WM tracts, including the bilateral inferior longitudinal fasciculi, bilateral inferior fronto-occipital fasciculi, and left uncinate fasciculus. Moreover, the patterns of FA and MD alterations were highly consistent with previous findings (Aoki et al., 2013; Vissers et al., 2012). On the other hand, linked ICA found two atypical components (#1 and #13) in participants with ASD. The spatial pattern of component #1 was similar to that reported in a previous study that used the same approach to examine the effect of age in a normal population (Groves et al., 2012); thus, this component may mainly reflect age-related changes in both groups. On the other hand, component #13 comprised decreased GM volumes in participants with ASD in distributed brain regions mainly in the bilateral fusiform gyri, bilateral superior temporal sulci, bilateral pre- and post-central gyri, and bilateral orbitofrontal cortices, as well as increased GM volumes in the bilateral lingual gyri, bilateral anterior temporal poles, bilateral putamen, and left superior frontal gyrus. This component also comprised decreased FA in participants with ASD mainly in the bilateral inferior longitudinal fasciculi, bilateral inferior fronto-occipital fasciculi, bilateral uncinate, fasciculi, and bilateral corticospinal tracts. Notably, this pattern of decreased FA in ASD substantially overlapped with that of reduced FA in ASD, as revealed by a unimodal analysis using TBSS. Importantly, these findings demonstrate the existence of co-occurring morphological alterations in specific brain networks of individuals with ASD, such as the one consisting of the right fusiform gyrus, right anterior temporal pole, and right orbitofrontal cortex; those could never be detected by conventional analysis. Therefore, the current study provides a comprehensive view for understanding the neuroanatomical anomalies of the ASD brain.

4.1. Abnormalities in GM morphology associated with ASD

Growing evidence from previous unimodal structural MRI studies suggests that people with ASD show altered GM morphology in both cortical and sub-cortical regions (see Cauda et al., 2011; Duerden et al., 2012; Nickl-Jockschat et al., 2012, for reviews). These alterations include decreased volumes in the right fusiform gyrus (Kwon et al., 2004), right insula, inferior frontal gyrus (Bonilha et al., 2008; Kosaka et al., 2010), and bilateral posterior superior temporal sulci (Greimel et al., 2013); increased volumes were found bilaterally in the pre- and post-central gyri (Ecker et al., 2012) and in the middle frontal gyri (Hyde et al., 2010). In the current study, however, volumetric between-group differences did not reach a significant level after the correction of multiple comparisons.

One possible reason for this discrepancy may be that the heterogeneity of ASD may obscure between-group differences. Indeed, morphological heterogeneity within the autism spectrum has been described in terms of systematic differences between Asperger's disorder and high-functioning autism (Kwon et al., 2004; McAlonan et al., 2008, 2009). In addition, the use of a relatively conservative statistical threshold (e.g., $p < 0.05$, family-wise error corrected for multiple comparisons) in this study might have failed to detect small but significant GM abnormalities in the ASD brain.

Recent neuroimaging studies have suggested that, instead of focusing on individual voxels, the use of multi-voxel pattern information may improve sensitivity to small changes (Norman et al., 2006) and relaxes correction for multiple comparisons. In order to confirm whether or not a multi-voxel pattern analysis can capture volumetric alterations that could not be detected by a unimodal VBM analysis, we applied probabilistic ICA (Beckmann and Smith, 2004) to GM data, which is also known as source-based morphometry (SBM; Xu et al., 2009). Notably, the ICA algorithm extracted a feature of ASD-related volume increases mainly in the posterior cingulate gyrus, right inferior frontal gyrus, and bilaterally in the superior temporal gyri (for details, see
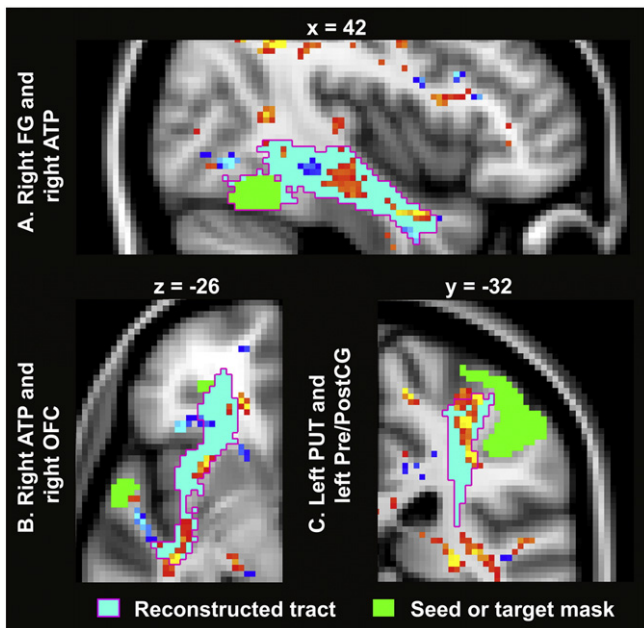
Section 1 in the Supplementary Material). Together with our findings for linked ICA, this observation suggests that, indeed, small morphological alterations in GM persist in adults with ASD and that, compared to univariate analyses, multivariate approaches may be more sensitive to small morphological abnormalities due to their exploitation of multi-voxel pattern information.

4.2. Abnormalities in WM structure associated with ASD

Previous DTI studies have reported that people with ASD show complex patterns of WM abnormalities along with development (see Travers et al., 2012, for an overview). Although, in general, adults with ASD tend to show FA reductions, there is still a lack of consistency among the reported findings. For example, some studies using tractography (Thomas et al., 2011) and TBSS (Bakhtiari et al., 2012) have reported no significant FA changes in adults with ASD, while other studies have reported FA reductions using the same procedures of tractography (Catani et al., 2008; Langen et al., 2012; Pugliese et al., 2009), voxel-based analysis (Bloemen et al., 2010; Keller et al., 2007), and TBSS (Gibbard et al., 2013; Kleinhans et al., 2012; Mueller et al., 2013). Our observation of widespread reductions in FA, along with increases in MD, especially in the bilateral inferior longitudinal fasciculi, left uncinate fasciculus, and bilateral corticospinal tracts (Fig. 1), provides further evidence in support of disrupted WM integrity in adults with ASD.

4.3. Co-occurrence of morphological alterations in ASD

Linked ICA revealed two components (#1 and #13) showing significant between-group differences in their shared component loadings. Notably, loading of component #1 was also associated with age, indicating that this component may represent age-related changes. In support of this view, Groves et al. (2012) reported a similar spatial pattern of global FA increases, accompanied by global MD decreases, and association between loading and age in that component. On the other hand, growing evidence suggests that the effect of aging in individuals with ASD differs from that in neurotypical individuals (e.g., Kleinhans et al., 2012). For component #1, the GM map encompassed multiple brain regions, such as the left superior temporal gyrus, bilateral putamen, left nucleus accumbens, and right hippocampus, some of which have been shown to follow different aging trajectories between NC and ASD (e.g., Greimel et al., 2013). Therefore, in conjunction with previous findings, our results indicate that component #1 may reflect atypical age-related changes in ASD, thereby leading to between-group difference in its loading.

Component #13 showed significant association in its loading only with diagnosis. This component encompassed several cortical regions (e.g., the bilateral fusiform gyri, bilateral anterior temporal poles, bilateral orbitofrontal cortices, and bilateral pre- and post-central gyri) in the GM map and WM tracts (e.g., the bilateral inferior longitudinal fasciculi, bilateral inferior fronto-occipital fasciculi, bilateral uncinate fasciculi, and bilateral corticospinal tracts) in the FA map. These cortical regions and WM tracts are implicated in brain functions including face perception (Cohen Kadosh and Johnson, 2007), integration of emotion with cognition and behavior (Catani et al., 2013), and motor controls (Stoodley et al., 2012), all of which are impaired in ASD.

Behaviorally, individuals with ASD are known to exhibit impairments related to face recognition, including abnormal emotional perception (Doyle-Thomas et al., 2013) and reduced attention to eyes (Sterling et al., 2008). Previous studies have hypothesized that impairments in face recognition may arise from a failure to transfer information from the fusiform face area to the anterior temporal pole through the inferior longitudinal fasciculus (Catani et al., 2003; Tavor et al., 2014). Consistent with this hypothesis, people with ASD show FA reductions in this tract (Bakhtiari et al., 2012; Jou et al., 2011; Kleinhans et al., 2012). Our analyses using TBSS and linked ICA are consistent with

previous findings in that significant FA reductions in the bilateral inferior longitudinal fasciculi were clearly identified in participants with ASD. In component #13, the GM map displayed significantly altered volumes in the right fusiform gyrus and the right anterior temporal pole (Fig. 4D). Furthermore, a cluster of voxels showing reduced FA values was observed on the reconstructed tract that might represent the right inferior longitudinal fasciculus (Fig. 5A). This finding provides further support from an independent imaging modality that disrupted connection between the right fusiform gyrus and right anterior temporal pole is present in individuals with ASD.

In addition to disrupted connection between the fusiform gyrus and anterior temporal pole, component #13 seems to include disruption on connection between the anterior temporal pole and orbitofrontal cortex, which is mediated by the uncinate fasciculus (Catani et al., 2002; Catani and Thiebaut de Schotten, 2008; Thiebaut de Schotten et al., 2012). This connection is known to play a critical role in integrating emotion with cognition and behavior (see Catani et al., 2013; for a review). Consistent with the results of our TBSS analysis and with previous DTI studies showing disruptions in this tract (Bakhtiari et al., 2012; Barnea-Goraly et al., 2010; Cheon et al., 2011; Jou et al., 2011; Kleinhans et al., 2012; Kumar et al., 2010; Pardini et al., 2009; Pugliese et al., 2009), our linked ICA revealed decreased FA in the left uncinate fasciculus in component #13 (Fig. 4A). In addition to disruption on the left uncinate fasciculus, our linked ICA and post-hoc tractography confirmed FA reductions on the connection between the right anterior temporal pole and right orbitofrontal cortex, which might represent a portion of the right uncinate fasciculus (Fig. 5B). In concurrence with recent meta-analytic studies of VBM (e.g., Cauda et al., 2011; Duerden et al., 2012), the GM map of this component also showed decreased volumes bilaterally in the orbitofrontal cortices (Fig. 4D). Taken together, component #13 may partially capture a disturbance of a large-scale network consisting of the bilateral orbitofrontal cortices, fusiform gyri, anterior temporal poles, and limbic regions, those of which are anatomically connected by the bilateral inferior longitudinal fasciculi, inferior fronto-occipital fasciculi, and uncinate fasciculi. In this study, we did not have behavioral data supporting the association of these abnormalities with specific behavioral characteristics in ASD. However, its disruptions may be responsible for atypical face perception (Kleinhans et al., 2008, 2011; Pierce et al., 2001) and impairments in integration of emotional states with cognition and behavior (Kamio et al., 2007; Schneider et al., 2013) in ASD.

It is noteworthy that component #13 also seems to include the motor network consisting of the bilateral primary sensorimotor cortices, and bilateral putamen (Fig. 4D). Post-hoc probabilistic tractography confirmed FA reductions on the connection between the left putamen and left pre- and post-central gyri, which might represent a portion of the left corticospinal tract (Fig. 5C). Although motor dysfunctions may not always be included in the core clinical symptoms of ASD, dyspraxia is frequently reported in people with this disorder (Dowell et al., 2009; Dziuk et al., 2007). As documented in previous functional imaging studies, individuals with ASD show atypical brain activation patterns during motor tasks (Mostofsky et al., 2009; Muller et al., 2004; Noonan et al., 2009; Takarae et al., 2007), and disrupted functional differentiation in the motor cortex, as indicated by resting-state fMRI data (Nebel et al., 2014). For instance, Mostofsky et al. (2009) reported decreased brain activation in the cerebellum and decreased functional connectivity between the bilateral thalamus and supplementary motor area during a motor task. Although we do not have fMRI evidence in the present study, our linked ICA findings suggest that morphological alterations in the motor network may underlie the impaired motor control and learning in individuals with ASD.

4.4. Methodological limitations and considerations

Several limitations should be considered for the appropriate interpretation of the present study. First, this study used a set of structural

measures (GM volume, FA, MD, and MO) as inputs. Although a previous study performed linked ICA using this combination (Groves et al., 2011), some readers may be concerned with the possibility of variable outputs depending on combinations of inputs (modalities). In order to validate the robustness of our findings, we fed a set of measures (FA, MD, and GM volume) into the linked ICA algorithm as inputs, thus excluding MO from the set (see Section 3 in the Supplementary Material). The linked ICA in this condition demonstrated that, although removal of MO broke component #13 into three components showing between-group differences in their loadings, the spatial pattern of component #13 basically was the same as that of the combination of those three components. In addition, some readers may be interested in whether the results are retained when the dimension of the linked ICA is reduced. In order to confirm the robustness of the results observed in the high-dimensional linked ICA (the number of components = 90), we set the number of independent components to 45 and ran a low-dimensional linked ICA on the same dataset. This analysis identified two composite components that showed significant between-group differences on their component loadings (see Section 4 in the Supplementary Material). One of the composite components exhibited a similar spatial pattern to component #13 involving GM alterations in the bilateral fusiform gyri and FA alterations in the bilateral inferior fronto-occipital fasciculi. This result confirms the robustness of the spatial patterns observed in the high-dimensional decomposition model.

Second, there are several other data-fusion analyses, including joint ICA (jICA; Calhoun et al., 2006), partial least square (PLS; Martinez-Montes et al., 2004), multi-set canonical correlation analysis (mCCA; Correa et al., 2010), parallel ICA (pICA; Liu et al., 2008, 2009), and the combination of mCCA and jICA (Sui et al., 2013a,b). Nonetheless, we chose the flat linked ICA among others in this study, because it has an advantage over other methods in that it requires a small number of assumptions on the spatial maps. On the other hand, other data-fusion approaches, such as jICA and tensor linked ICA (Groves et al., 2011), impose additional constraints (e.g., spatial alignment) on the spatial maps (Sui et al., 2012). Given the paucity of simulation studies that validate which assumptions are critical in data-fusion analyses, we determined to adopt a conservative approach that requires minimal explicit assumptions. Because the flat linked ICA involves fewer assumptions than other ICA-based data-fusion approaches (e.g., tensor linked ICA), we have decided that this approach would be suitable for our purpose. Future simulation studies will be needed to validate which assumptions are critical in data-fusion analyses.

Third, GM volume was used as one of the inputs in the linked ICA as a representative metric of GM tissue. The GM volume has an advantage in that it can be evaluated throughout the whole brain including subcortical structures such as the hippocampus and striatum in which significant structural alterations have been repeatedly demonstrated in individuals with ASD (e.g., Ecker et al., 2012). However, we acknowledge that, because the volume is a composite measure, the link with specific neurobiological factors (e.g., synaptic pruning) may be less clear compared with other possible measures such as cortical thickness or surface area (Jiang et al., 2009). Therefore, future studies using cortical thickness or surface measures may reveal more specific associations between GM and WM features at the cost of excluding subcortical structures from targets of investigation. Although it would be ideal to feed all the measures (i.e., GM volume, thickness, and surface area) into data-fusion analysis and exhaust every possible neuroanatomical linkage, the linked ICA, or multivariate data-driven approaches, requires a larger number of participants to capture patterns of latent inter-modal associations when increasing the number of modalities (or metrics). A previous linked ICA study used a large number of normal subjects ($n = 484$) to feed six structural and diffusion measures (GM density, thickness, surface area, FA, MD, and MO) (Groves et al., 2012). Whereas our study differs from that study in terms of sample size and the number of input features, the fact that component #1 in our study showed a

similar spatial pattern to the one reported by Groves et al. (Groves et al., 2012) supports the validity of our analysis. The inclusion of other measures awaits future investigation using a larger sample size.

Fourth, whereas we selected a linked ICA as the multimodal data-fusion analysis, it is also possible to explore the relationships among modalities after applying a standard ICA to each modality (i.e., a set of unimodal analyses). However, such an approach may present difficulties in the interpretability of results since it requires post-hoc correlational analyses in order to find associations between components obtained by separate ICA analyses. Some readers may be interested in whether the two different approaches (i.e., multimodal analysis and a set of unimodal analyses) capture similar inter-modal relationships or not. To explore the degree of similarity in component loadings captured by the two approaches, we used correlation analysis and evaluated associations between altered unimodal component loadings in each modality and altered shared loading of component #13. The correlation analysis revealed no significant associations, indicating that the two different approaches might capture different information in the given dataset (for details, see Section 2 in the Supplementary Material). Thus, at least for the dataset used in this study, linked ICA may be suitable for investigating associations between GM and WM morphology in terms of component loadings shared across modalities. However, future investigations will be needed to understand the exact relationships between the two approaches.

Fifth, the Edinburgh handedness score of the NC group was significantly higher than that of the ASD group ($p = 0.01$), consistent with several studies reporting an increased prevalence of left handedness in children with autism (Dane and Balci, 2007; Hauck and Dewey, 2001). To confirm whether our major findings would be retained after excluding the possible effects of handedness on brain structures, we repeated the second-level analyses of the loading matrix on all of the available participants while including age, TBV, and handedness as nuisance covariates. The results of these analyses demonstrated that the statistical conclusion was unchanged (#13: $t = 2.9$, $p = 0.005$, uncorrected). At the time of the MRI scans, 14 of the 46 participants with ASD were using one or more of medications (e.g., anti-depressant), and thus the medication might have affected the GM and WM morphology in the ASD group. To examine this possibility directly, we divided the ASD population into two groups (i.e., medicated ASD and non-medicated ASD), and we performed a one-way analysis of variance (ANOVA) on the component loading values in the three subject groups, including the NC group. We found a significant group effect ($F = 8.821$, $p < 0.001$). Furthermore, Tukey's post-hoc test demonstrated that, although the component loading of the NC group was significantly higher than that of the other two ASD groups ($p < 0.001$ for the medicated ASD group and $p = 0.048$ for the non-medicated ASD group), there was no significant difference between the medicated and non-medicated ASD groups ($p = 0.095$). Therefore, our statistical conclusions remain essentially unchanged regarding the linked ICA.

Sixth, we only included male participants in this study, because the prevalence of ASD is highly skewed towards the male population particularly among high-functioning individuals (Newschaffer et al., 2007). However, we do not intend to allege that our results are representative of the entire high-functioning ASD population, given the evidence for significant sexual dimorphism at many levels including cognition (Bolte et al., 2011), genetics (Gilman et al., 2011), and neuroanatomy (Beacher et al., 2012; Lai et al., 2013). Therefore, our results will need to be compared with future data-fusion studies that focus on female subjects in order to elucidate the patterns of linked anatomical alterations throughout the entire high-functioning ASD population.

Lastly, the ASD group in this study showed greater variability in their full-scale IQ scores compared to the NC group, while there was no significant difference between the two groups in terms of the mean IQ value ($p = 0.18$). Although it is a conventional practice in the field of ASD research that individuals with ASD whose IQs are higher than a

given threshold (usually 80) are all equally treated as "high-functioning," variations in general intelligence in this range among typically developed individuals are associated with morphometric changes in both GM and WM (Goh et al., 2011; Haasz et al., 2013; He et al., 2013). Therefore, in future studies, it will be necessary to control not only for the mean IQ, but also for the range and distribution of the IQs between groups. Furthermore, the IQ profile in high-functioning ASD shows a characteristic pattern containing both developed and underdeveloped domains (Kanai et al., 2012). It would be interesting to examine how such IQ profiles in ASD are associated with altered patterns of GM and WM.

5. Conclusion

In conclusion, this multimodal study highlighted that people with ASD showed co-occurred alterations in different aspects of brain morphology, suggesting the possibility that such morphological alterations might occur in specific brain networks associated with cognitive and affective functions. Our results not only provide a comprehensive view for understanding the neuroanatomy of ASD, but also indicate future research directions for revealing even deeper pathological mechanisms that cause such linkages of morphological abnormalities in people with ASD. Thus, methodological development of data-fusion approaches could pave the way towards finding new linkages between neuroanatomical abnormalities and cognitive behavioral impairments in people with ASD.

Supplementary data related to this article can be found online at http://doi.dx.org/10.1016/j.nicl.2014.11.019.

References

Ambrosi, E., Rossi-Espagnet, M.C., Kotzalidis, G.D., Comparelli, A., Del Casale, A., Carducci, F., Romano, A., Manfredi, G., Tatarelli, R., Bozzao, A., Girardi, P., 2013. Structural brain alterations in bipolar disorder II: a combined voxel-based morphometry (VBM) and diffusion tensor imaging (DTI) study. J. Affect. Disord. 150 (2), 610–615. http://dx.doi.org/10.1016/j.jad.2013.02.02323489395.

Andersson, J.L., Jenkinson, M., Smith, S., 2007. Non-Linear Registration, Aka Spatial Normalisation FMRIB Technical Report TR07JA2. FMRIB Analysis Group of the University of Oxford.

Aoki, Y., Abe, O., Nippashi, Y., Yamasue, H., 2013. Comparison of white matter integrity between autism spectrum disorder subjects and typically developing individuals: a meta-analysis of diffusion tensor imaging tractography studies. Mol. Autism 4 (1), 25. http://dx.doi.org/10.1186/2040-2392-4-2523876131.

Bakhtiari, R., Zürcher, N.R., Rogier, O., Russo, B., Hippolyte, L., Granziera, C., Araabi, B.N., Nili Ahmadabadi, M., Hadjikhani, N., 2012. Differences in white matter reflect atypical developmental trajectory in autism: a tract-based spatial statistics study. Neuroimage Clin. 1 (1), 48–56. http://dx.doi.org/10.1016/j.nicl.2012.09.00124179736.

Barnea-Goraly, N., Lotspeich, L.J., Reiss, A.L., 2010. Similar white matter aberrations in children with autism and their unaffected siblings: a diffusion tensor imaging study using tract-based spatial statistics. Arch. Gen. Psychiatry 67 (10), 1052–1060. http://dx.doi.org/10.1001/archgenpsychiatry.2010.12320921121.

Beacher, F.D., Minati, L., Baron-Cohen, S., Lombardo, M.V., Lai, M.C., Gray, M.A., Harrison, N.A., Critchley, H.D., 2012. Autism attenuates sex differences in brain structure: a combined voxel-based morphometry and diffusion tensor imaging study. A.J.N.R. Am. J. Neuroradiol. 33 (1), 83–89. http://dx.doi.org/10.3174/ajnr.A288022173769.

Beckmann, C.F., Smith, S.M., 2004. Probabilistic independent component analysis for functional magnetic resonance imaging. I. E.E.E. Trans. Med. Imaging 23 (2), 137–152. http://dx.doi.org/10.1109/TMI.2003.82282114964560.

Behrens, T.E., Berg, H.J., Jbabdi, S., Rushworth, M.F., Woolrich, M.W., 2007. Probabilistic diffusion tractography with multiple fibre orientations: what can we gain?

Neuroimage 34 (1), 144–155. http://dx.doi.org/10.1016/j.neuroimage.2006.09.01817070705.

Billeci, L., Calderoni, S., Tosetti, M., Catani, M., Muratori, F., 2012. White matter connectivity in children with autism spectrum disorders: a tract-based spatial statistics study. B.M.C. Neurol. 12, 148. http://dx.doi.org/10.1186/1471-2377-12-14823194030.

Bloemen, O.J., Deeley, Q., Sundram, F., Daly, E.M., Barker, G.J., Jones, D.K., van Amelsvoort, T.A., Schmitz, N., Robertson, D., Murphy, K.C., Murphy, D.G., 2010. White matter integrity in Asperger syndrome: a preliminary diffusion tensor magnetic resonance imaging study in adults. Autism Res. 3 (5), 203–213. http://dx.doi.org/10.1002/aur.14620625995.

Boddaert, N., Chabane, N., Gervais, H., Good, C.D., Bourgeois, M., Plumet, M.H., Barthélémy, C., Mouren, M.C., Artiges, E., Samson, Y., Brunelle, F., Frackowiak, R.S., Zilbovicius, M., 2004. Superior temporal sulcus anatomical abnormalities in childhood autism: a voxel-based morphometry MRI study. Neuroimage 23 (1), 364–369. http://dx.doi.org/10.1016/j.neuroimage.2004.06.01615325384.

Bölte, S., Duketis, E., Poustka, F., Holtmann, M., 2011. Sex differences in cognitive domains and their clinical correlates in higher-functioning autism spectrum disorders. Autism 15 (4), 497–511. http://dx.doi.org/10.1177/13623613103911621454389.

Bonilha, L., Cendes, F., Rorden, C., Eckert, M., Dalgalarrondo, P., Li, L.M., Steiner, C.E., 2008. Gray and white matter imbalance — typical structural abnormality underlying classic autism? Brain Dev. 30 (6), 396–401. http://dx.doi.org/10.1016/j.braindev.2007.11.00618362056.

Calhoun, V.D., Adali, T., Giuliani, N.R., Pekar, J.J., Kiehl, K.A., Pearlson, G.D., 2006. Method for multimodal analysis of independent source differences in schizophrenia: combining gray matter structural and auditory oddball functional data. Hum. Brain Mapp. 27 (1), 47–62. http://dx.doi.org/10.1002/hbm.2016616108017.

Catani, M., Dell'Acqua, F., Thiebaut de Schotten, M., 2013. A revised limbic system model for memory, emotion and behaviour. Neurosci. Biobehav. Rev. 37 (8), 1724–1737. http://dx.doi.org/10.1016/j.neubiorev.2013.07.00123850593.

Catani, M., Howard, R.J., Pajevic, S., Jones, D.K., 2002. Virtual in vivo interactive dissection of white matter fasciculi in the human brain. Neuroimage 17 (1), 77–94. http://dx.doi.org/10.1006/nimg.2002.113612482069.

Catani, M., Jones, D.K., Daly, E., Embiricos, N., Deeley, Q., Pugliese, L., Curran, S., Robertson, D., Murphy, D.G., 2008. Altered cerebellar feedback projections in Asperger syndrome. Neuroimage 41 (4), 1184–1191. http://dx.doi.org/10.1016/j.neuroimage.2008.03.04118495494.

Catani, M., Jones, D.K., Donato, R., Ffytche, D.H., 2003. Occipito-temporal connections in the human brain. Brain 126 (9), 2093–2107. http://dx.doi.org/10.1093/brain/awg20312821517.

Catani, M., Thiebaut de Schotten, M., 2008. A diffusion tensor imaging tractography atlas for virtual in vivo dissections. Cortex 44 (8), 1105–1132. http://dx.doi.org/10.1016/j.cortex.2008.05.00418619589.

Cauda, F., Geda, E., Sacco, K., D'Agata, F., Duca, S., Geminiani, G., Keller, R., 2011. Grey matter abnormality in autism spectrum disorder: an activation likelihood estimation meta-analysis study. J. Neurol. Neurosurg. Psychiatry 82 (12), 1304–1313. http://dx.doi.org/10.1136/jnnp.2010.23911121693631.

Cheon, K.A., Kim, Y.S., Oh, S.H., Park, S.Y., Yoon, H.W., Herrington, J., Nair, A., Koh, Y.J., Jang, D.P., Kim, Y.B., Leventhal, B.L., Cho, Z.H., Castellanos, F.X., Schultz, R.T., 2011. Involvement of the anterior thalamic radiation in boys with high functioning autism spectrum disorders: a diffusion tensor imaging study. Brain Res. 1417, 77–86. http://dx.doi.org/10.1016/j.brainres.2011.08.02021890117.

Cohen Kadosh, K., Johnson, M.H., 2007. Developing a cortex specialized for face perception. Trends Cogn. Sci. 11 (9), 367–369. http://dx.doi.org/10.1016/j.tics.2007.06.00717631408.

Comon, P., Jutten, C., 2010. Handbook of Blind Source Separation: Independent Component Analysis and Applications. Academic Press.

Correa, N.M., Eichele, T., Adali, T., Li, Y.O., Calhoun, V.D., 2010. Multi-set canonical correlation analysis for the fusion of concurrent single trial ERP and functional MRI. Neuroimage 50 (4), 1438–1445. http://dx.doi.org/10.1016/j.neuroimage.2010.01.06220100584.

Dane, S., Balci, N., 2007. Handedness, eyedness and nasal cycle in children with autism. Int. J. Dev. Neurosci. 25 (4), 223–226. http://dx.doi.org/10.1016/j.ijdevneu.2007.03.00517462849.

Douaud, G., Jbabdi, S., Behrens, T.E., Menke, R.A., Gass, A., Monsch, A.U., Rao, A., Whitcher, B., Kindlmann, G., Matthews, P.M., Smith, S., 2011. DTI measures in crossing-fibre areas: increased diffusion anisotropy reveals early white matter alteration in MCI and mild Alzheimer's disease. Neuroimage 55 (3), 880–890. http://dx.doi.org/10.1016/j.neuroimage.2010.12.08221182970.

Douaud, G., Smith, S., Jenkinson, M., Behrens, T., Johansen-Berg, H., Vickers, J., James, S., Voets, N., Watkins, K., Matthews, P.M., James, A., 2007. Anatomically related grey and white matter abnormalities in adolescent-onset schizophrenia. Brain 130 (9), 2375–2386. http://dx.doi.org/10.1093/brain/awm18417698497.

Dowell, L.R., Mahone, E.M., Mostofsky, S.H., 2009. Associations of postural knowledge and basic motor skill with dyspraxia in autism: implication for abnormalities in distributed connectivity and motor learning. Neuropsychol. 23 (5), 563–570. http://dx.doi.org/10.1037/a001564019702410.

Doyle-Thomas, K.A., Goldberg, J., Szatmari, P., Hall, G.B., 2013. Neurofunctional underpinnings of audiovisual emotion processing in teens with autism spectrum disorders. Front. Psychiatry 4, 48. http://dx.doi.org/10.3389/fpsyt.2013.0004823750139.

Duerden, E.G., Mak-Fan, K.M., Taylor, M.J., Roberts, S.W., 2012. Regional differences in grey and white matter in children and adults with autism spectrum disorders: an activation likelihood estimate (ALE) meta-analysis. Autism Res. 5 (1), 49–66. http://dx.doi.org/10.1002/aur.23522139976.

Dziuk, M.A., Gidley Larson, J.C., Apostu, A., Mahone, E.M., Denckla, M.B., Mostofsky, S.H., 2007. Dyspraxia in autism: association with motor, social, and communicative deficits. Dev. Med. Child Neurol. 49 (10), 734–739. http://dx.doi.org/10.1111/j.1469-8749.2007.00734.x17880641.

Ecker, C., Ginestet, C., Feng, Y., Johnston, P., Lombardo, M.V., Lai, M.C., Suckling, J., Palaniyappan, L., Daly, E., Murphy, C.M., Williams, S.C., Bullmore, E.T., Baron-Cohen, S., Brammer, M., Murphy, D.G., MRC AIMS Consortium, 2013. Brain surface anatomy in adults with autism: the relationship between surface area, cortical thickness, and autistic symptoms. JAMA Psychiatry 70 (1), 59–70. http://dx.doi.org/10.1001/jamapsychiatry.2013.26523404046.

Ecker, C., Suckling, J., Deoni, S.C., Lombardo, M.V., Bullmore, E.T., Baron-Cohen, S., Catani, M., Jezzard, P., Barnes, A., Bailey, A.J., Williams, S.C., Murphy, D.G., MRC AIMS Consortium, 2012. Brain anatomy and its relationship to behavior in adults with autism spectrum disorder: a multicenter magnetic resonance imaging study. Arch. Gen. Psychiatry 69 (2), 195–209. http://dx.doi.org/10.1001/archgenpsychiatry.2011.125122310506.

Ennis, D.B., Kindlmann, G., 2006. Orthogonal tensor invariants and the analysis of diffusion tensor magnetic resonance images. Magn. Reson. Med. 55 (1), 136–146. http://dx.doi.org/10.1002/mrm.2074116342267.

Ethofer, T., Gschwind, M., Vuilleumier, P., 2011. Processing social aspects of human gaze: a combined fMRI-DTI study. Neuroimage 55 (1), 411–419. http://dx.doi.org/10.1016/j.neuroimage.2010.11.03321095230.

Franco, A.R., Ling, J., Caprihan, A., Calhoun, V.D., Jung, R.E., Heileman, G.L., Mayer, A.R., 2008. Multimodal and multi-tissue measures of connectivity revealed by joint independent component analysis. I. E.E.E. J. Sel. Top. Signal Process. 2 (6), 986–997. http://dx.doi.org/10.1109/JSTSP.2008.200671819777078.

Gibbard, C.R., Ren, J., Seunarine, K.K., Clayden, J.D., Skuse, D.H., Clark, C.A., 2013. White matter microstructure correlates with autism trait severity in a combined clinical-control sample of high-functioning adults. Neuroimage Clin. 3, 106–114. http://dx.doi.org/10.1016/j.nicl.2013.07.00724179854.

Gilman, S.R., Iossifov, I., Levy, D., Ronemus, M., Wigler, M., Vitkup, D., 2011. Rare de novo variants associated with autism implicate a large functional network of genes involved in formation and function of synapses. Neuron 70 (5), 898–907. http://dx.doi.org/10.1016/j.neuron.2011.05.02121658583.

Goh, S., Bansal, R., Xu, D., Hao, X., Liu, J., Peterson, B.S., 2011. Neuroanatomical correlates of intellectual ability across the life span. Dev. Cogn. Neurosci. 1 (3), 305–312. http://dx.doi.org/10.1016/j.dcn.2011.03.00122436512.

Good, C.D., Johnsrude, I.S., Ashburner, J., Henson, R.N., Friston, K.J., Frackowiak, R.S., 2001. A voxel-based morphometric study of ageing in 465 normal adult human brains. Neuroimage 14 (1 1), 21–36. http://dx.doi.org/10.1006/nimg.2001.078611525331.

Greimel, E., Nehrkorn, B., Schulte-Rüther, M., Fink, G.R., Nickl-Jockschat, T., Herpertz-Dahlmann, B., Konrad, K., Eickhoff, S.B., 2013. Changes in grey matter development in autism spectrum disorder. Brain Struct. Funct. 218 (4), 929–942. http://dx.doi.org/10.1007/s00429-012-0439-922777602.

Groves, A.R., Beckmann, C.F., Smith, S.M., Woolrich, M.W., 2011. Linked independent component analysis for multimodal data fusion. Neuroimage 54 (3), 2198–2217. http://dx.doi.org/10.1016/j.neuroimage.2010.09.07320932919.

Groves, A.R., Smith, S.M., Fjell, A.M., Tamnes, C.K., Walhovd, K.B., Douaud, G., Woolrich, M.W., Westlye, L.T., 2012. Benefits of multi-modal fusion analysis on a large-scale dataset: life-span patterns of inter-subject variability in cortical morphometry and white matter microstructure. Neuroimage 63 (1), 365–380. http://dx.doi.org/10.1016/j.neuroimage.2012.06.03822750412.

Haász, J., Westlye, E.T., Fjær, S., Espeseth, T., Lundervold, A., Lundervold, A.J., 2013. General fluid-type intelligence is related to indices of white matter structure in middle-aged and old adults. Neuroimage 83, 372–383. http://dx.doi.org/10.1016/j.neuroimage.2013.06.04023791837.

Hadjikhani, N., Joseph, R.M., Snyder, J., Tager-Flusberg, H., 2006. Anatomical differences in the mirror neuron system and social cognition network in autism. Cereb. Cortex 16 (9), 1276–1282. http://dx.doi.org/10.1093/cercor/bhj06916306324.

Haller, S., Curtis, L., Badan, M., Bessero, S., Albom, M., Chantraine, F., Alimenti, A., Lovblad, K.O., Giannakopoulos, P., Merlo, M., 2013. Combined grey matter VBM and white matter TBSS analysis in young first episode psychosis patients with and without cannabis consumption. Brain Topogr. 26 (4), 641–647. http://dx.doi.org/10.1007/s10548-013-0288-823604786.

Hauck, J.A., Dewey, D., 2001. Hand preference and motor functioning in children with autism. J. Autism Dev. Disord. 31 (3), 265–277. http://dx.doi.org/10.1023/A:101079118978115518481.

He, Q., Xue, G., Chen, C., Chen, C., Lu, Z.L., Dong, Q., 2013. Decoding the neuroanatomical basis of reading ability: a multivoxel morphometric study. J. Neurosci. 33 (31), 12835–12843. http://dx.doi.org/10.1523/JNEUROSCI.0449-13.201323904618.

Hyde, K.L., Samson, F., Evans, A.C., Mottron, L., 2010. Neuroanatomical differences in brain areas implicated in perceptual and other core features of autism revealed by cortical thickness analysis and voxel-based morphometry. Hum. Brain Mapp. 31 (4), 556–566. http://dx.doi.org/10.1002/hbm.2088719790171.

Jacobs, H.I., Gronenschild, E.H., Evers, E.A., Ramakers, I.H., Hofman, P.A., Backes, W.H., Jolles, J., Verhey, F.R., Van Boxtel, M.P., 2012. Visuospatial processing in early Alzheimer's disease: a multimodal neuroimaging study. Cortex http://dx.doi.org/10.1016/j.cortex.2012.01.00522342463.

Jenkinson, M., Bannister, P., Brady, M., Smith, S., 2002. Improved optimization for the robust and accurate linear registration and motion correction of brain images. Neuroimage 17 (2), 825–841. http://dx.doi.org/10.1006/nimg.2002.113212377157.

Jenkinson, M., Smith, S., 2001. A global optimisation method for robust affine registration of brain images. Med. Image Anal. 5 (2), 143–156. http://dx.doi.org/10.1016/S1361-8415(01)00036-611516708.

Jiang, J., Zhu, W., Shi, F., Liu, Y., Li, J., Qin, W., Li, K., Yu, C., Jiang, T., 2009. Thick visual cortex in the early blind. J. Neurosci. 29 (7), 2205–2211. http://dx.doi.org/10.1523/JNEUROSCI.5451-08.200919228973.

Jones, D.K., 2004. The effect of gradient sampling schemes on measures derived from diffusion tensor MRI: a Monte Carlo study. Magn. Reson. Med. 51 (4), 807–815. http://dx.doi.org/10.1002/mrm.2003315065255.

Jou, R.J., Jackowski, A.P., Papademetris, X., Rajeevan, N., Staib, L.H., Volkmar, F.R., 2011. Diffusion tensor imaging in autism spectrum disorders: preliminary evidence of abnormal neural connectivity. Aust N ZJ. Psychiatry 45, 153–162.

Kamio, Y., Robins, D., Kelley, E., Swainson, B., Fein, D., 2007. Atypical lexical/semantic processing in high-functioning autism spectrum disorders without early language delay. J. Autism Dev. Disord. 37 (6), 1116–1122. http://dx.doi.org/10.1007/s10803-006-0254-317080275.

Kana, R.K., Libero, L.E., Hu, C.P., Deshpande, H.D., Colburn, J.S., 2014. Functional brain networks and white matter underlying theory-of-mind in autism. Soc. Cogn. Affect. Neurosci. 9 (1), 98–105. http://dx.doi.org/10.1093/scan/nss10622977198.

Kanai, C., Tani, M., Hashimoto, R., Yamada, T., Ota, H., Watanabe, H., Iwanami, A., Kato, N., 2012. Cognitive profiles of adults with Asperger's disorder, high-functioning autism, and pervasive developmental disorder not otherwise specified based on the WAIS-III. Res. Autism Spectr. Disord. 6, 58–64.

Keller, T.A., Kana, R.K., Just, M.A., 2007. A developmental study of the structural integrity of white matter in autism. Neuroreport 18 (1), 23–27. http://dx.doi.org/10.1097/01.wnr.0000239965.21685.9917259855.

Kleinhans, N.M., Pauley, G., Richards, T., Neuhaus, E., Martin, N., Corrigan, N.M., Shaw, D.W., Estes, A., Dager, S.R., 2012. Age-related abnormalities in white matter microstructure in autism spectrum disorders. Brain Res. 1479, 1–16. http://dx.doi.org/10.1016/j.brainres.2012.07.05622902768.

Kleinhans, N.M., Richards, T., Johnson, L.C., Weaver, K.E., Greenson, J., Dawson, G., Aylward, E., 2011. fMRI evidence of neural abnormalities in the subcortical face processing system in ASD. Neuroimage 54 (1), 697–704. http://dx.doi.org/10.1016/j.neuroimage.2010.07.03720656041.

Kleinhans, N.M., Richards, T., Sterling, L., Stegbauer, K.C., Mahurin, R., Johnson, L.C., Greenson, J., Dawson, G., Aylward, E., 2008. Abnormal functional connectivity in autism spectrum disorders during face processing. Brain 131 (4), 1000–1012. http://dx.doi.org/10.1093/brain/awm33418234695.

Kosaka, H., Omori, M., Munesue, T., Ishitobi, M., Matsumura, Y., Takahashi, T., Narita, K., Murata, T., Saito, D.N., Uchiyama, H., Morita, T., Kikuchi, M., Mizukami, K., Okazawa, H., Sadato, N., Wada, Y., 2010. Smaller insula and inferior frontal Volumes in young adults with pervasive developmental disorders. Neuroimage 50 (4), 1357–1363. http://dx.doi.org/10.1016/j.neuroimage.2010.01.08520123027.

Kumar, A., Sundaram, S.K., Sivaswamy, L., Behen, M.E., Makki, M.I., Ager, J., Janisse, J., Chugani, H.T., Chugani, D.C., 2010. Alterations in frontal lobe tracts and corpus callosum in young children with autism spectrum disorder. Cereb. Cortex 20 (9), 2103–2113. http://dx.doi.org/10.1093/cercor/bhp27820019145.

Kwon, H., Ow, A.W., Pedatella, K.E., Lotspeich, L.J., Reiss, A.L., 2004. Voxel-based morphometry elucidates structural neuroanatomy of high-functioning autism and Asperger syndrome. Dev. Med. Child Neurol. 46 (11), 760–76415540637.

Lai, M.C., Lombardo, M.V., Suckling, J., Ruigrok, A.N., Chakrabarti, B., Ecker, C., Deoni, S.C., Craig, M.C., Murphy, D.G., Bullmore, E.T., MRC AIMS Consortium, 2013. Biological sex affects the neurobiology of autism. Brain 136 (9), 2799–2815. http://dx.doi.org/10.1093/brain/awt21623935125.

Langen, M., Leemans, A., Johnston, P., Ecker, C., Daly, E., Murphy, C.M., Dell'acqua, F., Durston, S., AIMS Consortium, Murphy, D.G., 2012. Fronto-striatal circuitry and inhibitory control in autism: findings from diffusion tensor imaging tractography. Cortex 48 (2), 183–193. http://dx.doi.org/10.1016/j.cortex.2011.05.01821718979.

Lerch, J.P., Worsley, K., Shaw, W.P., Greenstein, D.K., Lenroot, R.K., Giedd, J., Evans, A.C., 2006. Mapping anatomical correlations across cerebral cortex (MACACC) using cortical thickness from MRI. Neuroimage 31 (3), 993–1003. http://dx.doi.org/10.1016/j.neuroimage.2006.01.04216624590.

Li, Y., Wang, Y., Hu, Y., Liang, Y., Chen, F., 2013. Structural changes in left fusiform areas and associated fiber connections in children with abacus training: evidence from morphometry and tractography. Front. Hum. Neurosci. 7, 335. http://dx.doi.org/10.3389/fnhum.2013.0033523847506.

Liu, J., Demirci, O., Calhoun, V.D., 2008. A parallel independent component analysis approach to investigate genomic influence on brain function. I. E.E.E. Signal Process. Lett. 15, 413–416. http://dx.doi.org/10.1109/LSP.2008.92251319834575.

Liu, J., Pearlson, G., Windemuth, A., Ruano, G., Perrone-Bizzozero, N.I., Calhoun, V., 2009. Combining fMRI and SNP data to investigate connections between brain function and genetics using parallel ICA. Hum. Brain Mapp. 30 (1), 241–255. http://dx.doi.org/10.1002/hbm.2050818072279.

Lord, C., Risi, S., Lambrecht, L., Cook Jr., E.H., Leventhal, B.L., DiLavore, P.C., Pickles, A., Rutter, M., 2000. The autism diagnostic observation schedule-generic: a standard measure of social and communication deficits associated with the spectrum of autism. J. Autism Dev. Disord. 30 (3), 205–223. http://dx.doi.org/10.1023/A:100559240194711055457.

Maljaars, J., Noens, I., Scholte, E., van Berckelaer-Onnes, I., 2012. Evaluation of the criterion and convergent validity of the diagnostic interview for social and communication disorders in young and low-functioning children. Autism 16 (5), 487–497. http://dx.doi.org/10.1177/1362361311140285721690082.

Mangalathu-Arumana, J., Beardsley, S.A., Liebenthal, E., 2012. Within-subject joint independent component analysis of simultaneous fMRI/ERP in an auditory oddball paradigm. Neuroimage 60 (4), 2247–2257. http://dx.doi.org/10.1016/j.neuroimage.2012.02.03022377443.

Martínez-Montes, E., Valdés-Sosa, P.A., Miwakeichi, F., Goldman, R.I., Cohen, M.S., 2004. Concurrent EEG/fMRI analysis by multiway partial least squares. Neuroimage 22 (3), 1023–1034. http://dx.doi.org/10.1016/j.neuroimage.2004.03.03815291975.

Matsuoka, K., Uno, M., Kasai, K., Koyama, K., Kim, Y., 2006. Estimation of premorbid IQ in individuals with Alzheimer's disease using Japanese ideographic script (Kanji) compound words: Japanese version of National Adult Reading Test. Psychiatry Clin. Neurosci. 60 (3), 332–339. http://dx.doi.org/10.1111/j.1440-1819.2006.01510.x16732750.

McAlonan, G.M., Cheung, C., Cheung, V., Wong, N., Suckling, J., Chua, S.E., 2009. Differential effects on white-matter systems in high-functioning autism and Asperger's syndrome. Psychol. Med. 39 (11), 1885–1893. http://dx.doi.org/10.1017/S003329170900572819356262.

McAlonan, G.M., Suckling, J., Wong, N., Cheung, V., Lienenkaemper, N., Cheung, C., Chua, S.E., 2008. Distinct patterns of grey matter abnormality in high-functioning autism and Asperger's syndrome. J. Child Psychol. Psychiatry 49 (12), 1287–1295. http://dx.doi.org/10.1111/j.1469-7610.2008.01933.x18673405.

Mengotti, P., D'Agostini, S., Terlevic, R., De Colle, C., Biasizzo, E., Londero, D., Ferro, A., Rambaldelli, G., Balestrieri, M., Zanini, S., Fabbro, F., Molteni, M., Brambilla, P., 2011. Altered white matter integrity and development in children with autism: a combined voxel-based morphometry and diffusion imaging study. Brain Res. Bull. 84 (2), 189–195. http://dx.doi.org/10.1016/j.brainresbull.2010.12.00221146593.

Mostofsky, S.H., Powell, S.K., Simmonds, D.J., Goldberg, M.C., Caffo, B., Pekar, J.J., 2009. Decreased connectivity and cerebellar activity in autism during motor task performance. Brain 132 (9), 2413–2425. http://dx.doi.org/10.1093/brain/awp08819389870.

Mueller, S., Keeser, D., Samson, A.C., Kirsch, V., Blautzik, J., Grothe, M., Erat, O., Hegenloh, M., Coates, U., Reiser, M.F., Hennig-Fast, K., Meindl, T., 2013. Convergent findings of altered functional and structural brain connectivity in individuals with high functioning autism: a multimodal MRI study. PLOS One 8 (6), e67329. http://dx.doi.org/10.1371/journal.pone.006732923825652.

Müller, R.A., Cauich, C., Rubio, M.A., Mizuno, A., Courchesne, E., 2004. Abnormal activity patterns in premotor cortex during sequence learning in autistic patients. Biol. Psychiatry 56 (5), 323–332. http://dx.doi.org/10.1016/j.biopsych.2004.06.00715336514.

Nebel, M.B., Joel, S.E., Muschelli, J., Barber, A.D., Caffo, B.S., Pekar, J.J., Mostofsky, S.H., 2014. Disruption of functional organization within the primary motor cortex in children with autism. Hum. Brain Mapp. 35, 567–580. http://dx.doi.org/10.1002/hbm.2218823118015.

Newschaffer, C.J., Croen, L.A., Daniels, J., Giarelli, E., Grether, J.K., Levy, S.E., Mandell, D.S., Miller, L.A., Pinto-Martin, J., Reaven, J., Reynolds, A.M., Rice, C.E., Schendel, D., Windham, G.C., 2007. The epidemiology of autism spectrum disorders. Annu. Rev. Public Health 28, 235–258. http://dx.doi.org/10.1146/annurev.publhealth.28.021406.14400717367287.

Nickl-Jockschat, T., Habel, U., Michel, T.M., Manning, J., Laird, A.R., Fox, P.T., Schneider, F., Eickhoff, S.B., 2012. Brain structure anomalies in autism spectrum disorder — a meta-analysis of VBM studies using anatomic likelihood estimation. Hum. Brain Mapp. 33 (6), 1470–1489. http://dx.doi.org/10.1002/hbm.2129921692142.

Noonan, S.K., Haist, F., Müller, R.A., 2009. Aberrant functional connectivity in autism: evidence from low-frequency BOLD signal fluctuations. Brain Res. 1262, 48–63. http://dx.doi.org/10.1016/j.brainres.2008.12.07619401185.

Norman, K.A., Polyn, S.M., Detre, G.J., Haxby, J.V., 2006. Beyond mind-reading: multi-voxel pattern analysis of fMRI data. Trends Cogn. Sci. 10 (9), 424–430. http://dx.doi.org/10.1016/j.tics.2006.07.00516899397.

Oguz, I., Farzinfar, M., Matsui, J., Budin, F., Liu, Z., Gerig, G., Johnson, H.J., Styner, M., 2014. DTIPrep: quality control of diffusion-weighted images. Front. Neuroinform 8, 4. http://dx.doi.org/10.3389/fninf.2014.0000424523693.

Oldfield, R.C., 1971. The assessment and analysis of handedness: the Edinburgh inventory. Neuropsychologia 9 (1), 97–113. http://dx.doi.org/10.1016/0028-3932(71)90067-45146491.

Papadakis, N.G., Murrills, C.D., Hall, L.D., Huang, C.L., Adrian Carpenter, T., 2000. Minimal gradient encoding for robust estimation of diffusion anisotropy. Magn. Reson. Imaging 18 (6), 671–679. http://dx.doi.org/10.1016/S0730-725X(00)00151-X10930776.

Pardini, M., Garaci, F.G., Bonzano, L., Roccatagliata, L., Palmieri, M.G., Pompili, E., Coniglione, F., Krueger, F., Ludovici, A., Floris, R., Benassi, F., Emberti Gialloreti, L., 2009. White matter reduced streamline coherence in young men with autism and mental retardation. Eur. J. Neurol. 16 (11), 1185–1190. http://dx.doi.org/10.1111/j.1468-1331.2009.02699.x19538216.

Pascual-Leone, A., Amedi, A., Fregni, F., Merabet, L.B., 2005. The plastic human brain cortex. Annu. Rev. Neurosci. 28, 377–401. http://dx.doi.org/10.1146/annurev.neuro.27.070203.14421616022601.

Pezawas, L., Verchinski, B.A., Mattay, V.S., Callicott, J.H., Kolachana, B.S., Straub, R.E., Egan, M.F., Meyer-Lindenberg, A., Weinberger, D.R., 2004. The brain-derived neurotrophic factor val66met polymorphism and variation in human cortical morphology. J. Neurosci. 24 (45), 10099–10102. http://dx.doi.org/10.1523/JNEUROSCI.2680-04.200415537879.

Pierce, K., Müller, R.A., Ambrose, J., Allen, G., Courchesne, E., 2001. Face processing occurs outside the fusiform 'face area' in autism: evidence from functional MRI. Brain 124 (10), 2059–2073. http://dx.doi.org/10.1093/brain/124.10.205911571222.

Pugliese, L., Catani, M., Ameis, S., Dell'Acqua, F., Thiebaut de Schotten, M., Murphy, C., Robertson, D., Deeley, Q., Daly, E., Murphy, D.G., 2009. The anatomy of extended limbic pathways in Asperger syndrome: a preliminary diffusion tensor imaging tractography study. Neuroimage 47 (2), 427–434. http://dx.doi.org/10.1016/j.neuroimage.2009.05.01419446642.

Quinque, E.M., Arélin, K., Dukart, J., Roggenhofer, E., Streitbuerger, D.P., Villringer, A., Frisch, S., Mueller, K., Schroeter, M.L., 2012. Identifying the neural correlates of executive functions in early cerebral microangiopathy: a combined VBM and DTI study. J. Cereb. Blood Flow Metab. 32 (10), 1869–1878. http://dx.doi.org/10.1038/jcbfm.2012.9622781332.

Rojas, D.C., Peterson, E., Winterrowd, E., Reite, M.L., Rogers, S.J., Tregellas, J.R., 2006. Regional gray matter volumetric changes in autism associated with social and repetitive behavior symptoms. B.M.C. Psychiatry 6, 56. http://dx.doi.org/10.1186/1471-244X-6-5617166273.

Ruef, A., Curtis, L., Moy, G., Bessero, S., Badan Bâ, M., Lazeyras, F., Lövblad, K.O., Haller, S., Malafosse, A., Giannakopoulos, P., Merlo, M., 2012. Magnetic resonance imaging correlates of first-episode psychosis in young adult male patients: combined analysis of grey and white matter. J. Psychiatry Neurosci. 37 (5), 305–312. http://dx.doi.org/10.1503/jpn.11005722748698.

Schlösser, R.G., Nenadic, I., Wagner, G., Güllmar, D., von Consbruch, K., Köhler, S., Schultz, C.C., Koch, K., Fitzek, C., Matthews, P.M., Reichenbach, J.R., Sauer, H., 2007. White matter abnormalities and brain activation in schizophrenia: a combined DTI and fMRI study. Schizophr. Res. 89 (1–3), 1–11. http://dx.doi.org/10.1016/j.schres.2006.09.00717085018.

Schneider, K., Pauly, K.D., Gossen, A., Mevissen, L., Michel, T.M., Gur, R.C., Schneider, F., Habel, U., 2013. Neural correlates of moral reasoning in autism spectrum disorder. Soc. Cogn. Affect. Neurosci. 8 (6), 702–710. http://dx.doi.org/10.1093/scan/nss05122569187.

Smith, S.M., Jenkinson, M., Johansen-Berg, H., Rueckert, D., Nichols, T.E., Mackay, C.E., Watkins, K.E., Ciccarelli, O., Cader, M.Z., Matthews, P.M., Behrens, T.E., 2006. Tract-based spatial statistics: voxelwise analysis of multi-subject diffusion data. Neuroimage 31 (4), 1487–1505. http://dx.doi.org/10.1016/j.neuroimage.2006.02.02416624579.

Smith, S.M., Jenkinson, M., Woolrich, M.W., Beckmann, C.F., Behrens, T.E., Johansen-Berg, H., Bannister, P.R., De Luca, M., Drobnjak, I., Flitney, D.E., Niazy, R.K., Saunders, J., Vickers, J., Zhang, Y., De Stefano, N., Brady, J.M., Matthews, P.M., 2004. Advances in functional and structural MR image analysis and implementation as FSL. Neuroimage 23 (Suppl. 1), S208–S219. http://dx.doi.org/10.1016/j.neuroimage.2004.07.05115501092.

Smith, S.M., Nichols, T.E., 2009. Threshold-free cluster enhancement: addressing problems of smoothing, threshold dependence and localisation in cluster inference. Neuroimage 44 (1), 83–98. http://dx.doi.org/10.1016/j.neuroimage.2008.03.06118501637.

Smith, S.M., Zhang, Y., Jenkinson, M., Chen, J., Matthews, P.M., Federico, A., De Stefano, N., 2002. Accurate, robust, and automated longitudinal and cross-sectional brain change analysis. Neuroimage 17 (1), 479–489. http://dx.doi.org/10.1006/nimg.2002.104012482100.

Sterling, L., Dawson, G., Webb, S., Murias, M., Munson, J., Panagiotides, H., Aylward, E., 2008. The role of face familiarity in eye tracking of faces by individuals with autism spectrum disorders. J. Autism Dev. Disord. 38 (9), 1666–1675. http://dx.doi.org/10.1007/s10803-008-0550-118306030.

Stoodley, C.J., Valera, E.M., Schmahmann, J.D., 2012. Functional topography of the cerebellum for motor and cognitive tasks: an fMRI study. Neuroimage 59 (2), 1560–1570. http://dx.doi.org/10.1016/j.neuroimage.2011.08.06521907811.

Storey, J.D., 2002. A direct approach to false discovery rates. J. R. Stat. Soc. B. Stat. Methodol. 64, 479–498.

Sui, J., Adali, T., Yu, Q., Chen, J., Calhoun, V.D., 2012. A review of multivariate methods for multimodal fusion of brain imaging data. J. Neurosci. Methods 204 (1), 68–81. http://dx.doi.org/10.1016/j.jneumeth.2011.10.031.

Sui, J., He, H., Pearlson, G.D., Adali, T., Kiehl, K.A., Yu, Q., Clark, V.P., Castro, E., White, T., Mueller, B.A., Ho, B.C., Andreasen, N.C., Calhoun, V.D., 2013a. Three-way (N-way) fusion of brain imaging data based on mCCA + jICA and its application to discriminating schizophrenia. Neuroimage 66, 119–132. http://dx.doi.org/10.1016/j.neuroimage.2012.10.05123108278.

Sui, J., He, H., Yu, Q., Chen, J., Rogers, J., Pearlson, G.D., Mayer, A., Bustillo, J., Canive, J., Calhoun, V.D., 2013b. Combination of resting state fMRI, DTI, and sMRI data to discriminate schizophrenia by N-way MCCA + jICA. Front. Hum. Neurosci. 7, 235. http://dx.doi.org/10.3389/fnhum.2013.0023523755002.

Sui, J., Huster, R., Yu, Q., Segall, J.M., Calhoun, V.D., 2013c. Function–structure associations of the brain: evidence from multimodal connectivity and covariance studies. Neuroimage http://dx.doi.org/10.1016/j.neuroimage.2013.09.04424084066.

Sui, J., Pearlson, G., Caprihan, A., Adali, T., Kiehl, K.A., Liu, J., Yamamoto, J., Calhoun, V.D., 2011. Discriminating schizophrenia and bipolar disorder by fusing fMRI and DTI in a multimodal CCA+ joint ICA model. Neuroimage 57 (3), 839–855. http://dx.doi.org/10.1016/j.neuroimage.2011.05.05521640835.

Takarae, Y., Minshew, N.J., Luna, B., Sweeney, J.A., 2007. Atypical involvement of frontostriatal systems during sensorimotor control in autism. Psychiatry Res. 156 (2), 117–127. http://dx.doi.org/10.1016/j.pscychresns.2007.03.00817913474.

Tavor, I., Yablonski, M., Mezer, A., Rom, S., Assaf, Y., Yovel, G., 2014. Separate parts of occipito-temporal white matter fibers are associated with recognition of faces and places. Neuroimage 86, 123–130. http://dx.doi.org/10.1016/j.neuroimage.2013.07.08523933304.

Teipel, S.J., Bokde, A.L., Meindl, T., Amaro Jr., E., Soldner, J., Reiser, M.F., Herpertz, S.C., Möller, H.J., Hampel, H., 2010. White matter microstructure underlying default mode network connectivity in the human brain. Neuroimage 49 (3), 2021–2032. http://dx.doi.org/10.1016/j.neuroimage.2009.10.06719878723.

Thiebaut de Schotten, M., Dell'Acqua, F., Valabregue, R., Catani, M., 2012. Monkey to human comparative anatomy of the frontal lobe association tracts. Cortex 48 (1), 82–96. http://dx.doi.org/10.1016/j.cortex.2011.10.00122088488.

Thomas, C., Humphreys, K., Jung, K.J., Minshew, N., Behrmann, M., 2011. The anatomy of the callosal and visual-association pathways in high-functioning autism: a DTI tractography study. Cortex 47 (7), 863–873. http://dx.doi.org/10.1016/j.cortex.2010.07.00620832784.

Travers, B.G., Adluru, N., Ennis, C., Tromp, Do P.M., Destiche, D., Doran, S., Bigler, E.D., Lange, N., Lainhart, J.E., Alexander, A.L., 2012. Diffusion tensor imaging in autism spectrum disorder: a review. Autism Res. 5 (5), 289–313. http://dx.doi.org/10.1002/aur.124322786754.

Vissers, M.E., Cohen, M.X., Geurts, H.M., 2012. Brain connectivity and high functioning autism: a promising path of research that needs refined models, methodological convergence, and stronger behavioral links. Neurosci. Biobehav. Rev. 36 (1), 604–625. http://dx.doi.org/10.1016/j.neubiorev.2011.09.00321963441.

Waiter, G.D., Williams, J.H., Murray, A.D., Gilchrist, A., Perrett, D.I., Whiten, A., 2004. A voxel-based investigation of brain structure in male adolescents with autistic

spectrum disorder. Neuroimage 22 (2), 619–625. http://dx.doi.org/10.1016/j.neuroimage.2004.02.02915193590.

Wakabayashi, A., Baron-Cohen, S., Wheelwright, S., Tojo, Y., 2006. The autism-Spectrum quotient (AQ) in Japan: a cross-cultural comparison. J. Autism Dev. Disord. 36 (2), 263–270. http://dx.doi.org/10.1007/s10803-005-0061-216586157.

Weinstein, M., Ben-Sira, L., Levy, Y., Zachor, D.A., Ben Itzhak, E., Artzi, M., Tarrasch, R., Eksteine, P.M., Hendler, T., Ben Bashat, D., 2011. Abnormal white matter integrity in young children with autism. Hum. Brain Mapp. 32 (4), 534–543. http://dx.doi.org/10.1002/hbm.2104221391246.

Wing, L., Leekam, S.R., Libby, S.J., Gould, J., Larcombe, M., 2002. The diagnostic interview for social and communication disorders: background, inter-rater reliability and clinical use. J. Child Psychol. Psychiatry 43 (3), 307–325. http://dx.doi.org/10.1111/1469-7610.0002311944874.

Xu, L., Groth, K.M., Pearlson, G., Schretlen, D.J., Calhoun, V.D., 2009. Source-based morphometry: the use of independent component analysis to identify gray matter differences with application to schizophrenia. Hum. Brain Mapp. 30 (3), 711–724. http://dx.doi.org/10.1002/hbm.2054018266214.

Zhang, Y., Brady, M., Smith, S., 2001. Segmentation of brain MR images through a hidden Markov random field model and the expectation–maximization algorithm. I. E.E.E. Trans. Med. Imaging 20 (1), 45–57. http://dx.doi.org/10.1109/42.90642411293691.